 https://doi.org/10.3311/PPee.36760

Periodica Polytechnica Electrical Engineering and Computer Science, 68(4), pp. 392–412, 2024

Improved Power Control Based Variable Speed Wind-Turbine DFIG under Hard Work Conditions: Application of Sliding Mode Theory

Hichem Itouchene[1*], Zoubir Boudries[1], Fayssal Amrane[2]

[1] Laboratoire de Technologie Industrielle et de l'Information (LTII), Faculté de Technologie, Université de Bejaia, 06000 Bejaia, Algeria
[2] LAS Research Laboratory, Department of Electrical Engineering, Setif-1 University Ferhat ABBAS, 19000 Setif, Algeria
[*] Corresponding author, e-mail: hichem.itouchene@univ-bejaia.dz

Received: 28 February 2024, Accepted: 08 August 2024, Published online: 11 September 2024

Abstract

This paper introduces an efficient and simple power control for the Wind Energy Conversion System (WECS) based on the Doubly-Fed Induction Generator (DFIG). Due to the limitation performance of the conventional PI controller against DFIG parameters change and wind speed variation; the sliding mode theory is applied in order to overcome these drawbacks. To improve the performances of a WECS, robust and nonlinear control techniques, namely; Conventional Sliding Mode Control (C-SMC) and Third Order Sliding Mode Control (3O-SMC), were implemented to independently control the stator active and reactive powers. However, both techniques exhibited a chattering phenomenon, an undesirable phenomenon caused by discontinuous signals. To overcome this drawback and further enhance previous control techniques, an advanced Variable Gain Super Twisting Algorithm (VGSTA) is proposed and compared to SMC and 3O-SMC. Furthermore, to validate the effectiveness of the proposed VGSTA strategy in comparison to two previous control methods, the WECS was simulated and validates using the MATLAB/Simulink environment. The simulation results clearly demonstrated the superiority of the proposed VGSTA strategy over the previous SMC and 3O-SMC techniques. This was obvious in terms of both fast convergence velocity and reduce chattering phenomenon.

Keywords

Sliding Mode Control (SMC), Third Order Sliding Mode Control (3O-SMC), Variable Gain Super Twisting Algorithm (VGSTA), Doubly Fed Induction Generator (DFIG), chattering phenomenon, nonlinear control, Rotor Side Converter (RSC)

1 Introduction

With the growing awareness of environmental problems arising from the use of fossil fuels and the projected rise in energy consumption in the coming decades, many countries have embarked on a quest to identify optimal methods of energy production [1]. In recent years, governments worldwide have recognized renewable energy as a viable alternative to polluting energy sources [2, 3] due to its ability to ensure energy autonomy for all nations [4, 5]. An unprecedented global challenge is being launched today in the field of energy resources. In this context, there are several forms of renewable energy. Wind energy is considered one of the most important sources of renewable energy, as it ranks second after hydropower [6]. Wind turbine technology has become a highly promising, reliable, and clean source of renewable energy [7]. The use of Wind Energy Conversion Systems (WECS) based on Doubly-Fed Induction Generators (DFIG) has gained significant popularity in different generations of wind energy systems. This technology has found widespread adoption, especially in remote and rural areas, owing to its numerous advantages that are highly relevant in the present era [8, 9].

In the WECS review based DFIG, the stator is directly connected to the grid, while the rotor is connected to the grid through back-to-back converters, as shown in the provided Fig. 1. The control of the DC link voltage and the stator powers (P_s and Q_s) is accomplished by the grid-side converter (GSC) and the rotor-side converter (RSC) respectively [10]. Robust control is a critical aspect of renewable energy technologies, particularly in dealing with external disturbances, uncertainties, and nonlinearities in nonlinear systems such as WEC Systems [11]. In the literature, many discussions have taken place regarding numerous

Cite this article as: Itouchene, H., Boudries, Z., Amrane, F. "Improved Power Control Based Variable Speed Wind-Turbine DFIG under Hard Work Conditions: Application of Sliding Mode Theory", Periodica Polytechnica Electrical Engineering and Computer Science, 68(4), pp. 392–412, 2024. https://doi.org/10.3311/PPee.36760

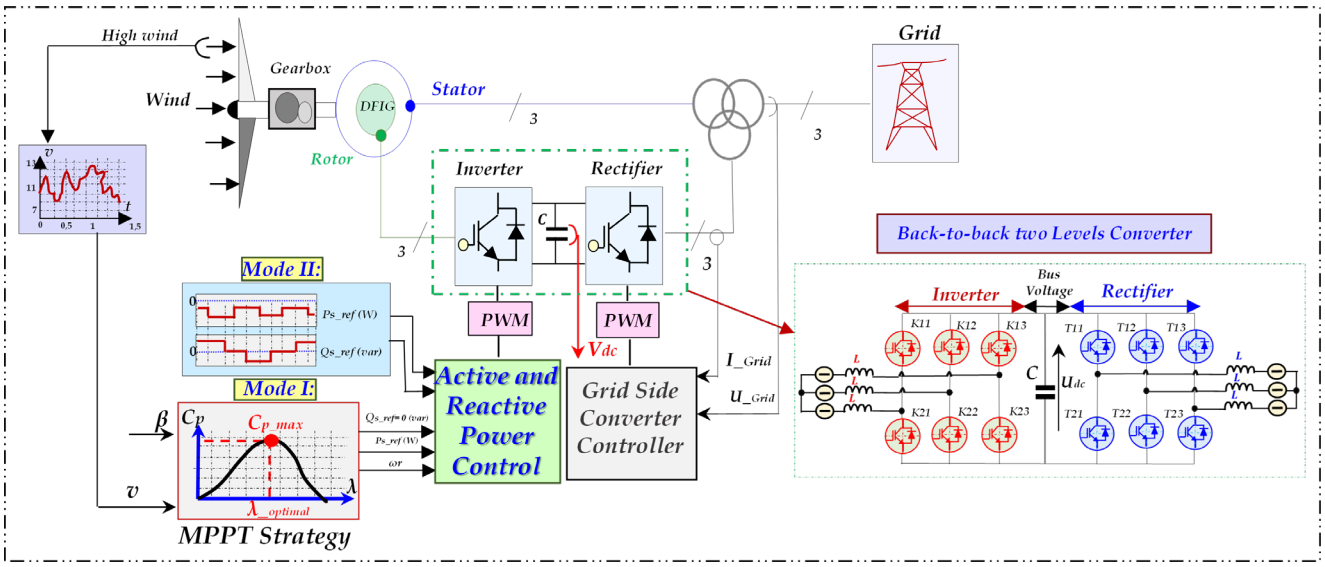

Fig. 1 The WEC System including: turbine, gearbox, generator, filter, converters, MPPT control, transformer and grid

control strategies for DFIG systems. These control strategies include Direct Torque Control (DTC) [12, 13], Model Reference Adaptive Control (MRAC) [14, 15], Model Reference Adaptive System (MRAS) [16–20], and Backstepping [21–23]. These discussions have significantly contributed to the advancement of knowledge in the field. They assist researchers, engineers, and practitioners in making informed decisions regarding the selection and implementation of control strategies for DFIG systems.

In recent years, Sliding Mode Control (SMC) has gained significant popularity; particularly in nonlinear systems (refer Fig. 2). Many researchers have explored robust control systems that incorporate a discontinuous control signal through a sliding surface to satisfy the sliding condition [24]. Nevertheless, standard SMC has a notable drawback, which is the chattering phenomenon that can be detrimental to the system [25]. This phenomenon is caused by the discontinuous signals introduced by the sign function [26].

In [10, 27] provided a detailed Super Twisting Sliding Mode Control (ST-SMC) strategy for a DFIG, enabling independent control of the active and reactive stator powers. In [26], the authors proposed the super twisting fractional order terminal sliding mode control (ST-FOTSMC) strategy to address the chattering phenomenon associated with classical SMC control. Moreover, in [28], a novel strategy for Direct Field-Oriented Control (DFOC) was developed utilizing third-order sliding mode (3O-SM). Control to minimize oscillations and reduce Total Harmonic Distortion (THD) in the current and active power of induction generators. Furthermore, the use of Fractional Calculus theory (FCT) to enhance the Super-Twisting Algorithm (STA) to achieve

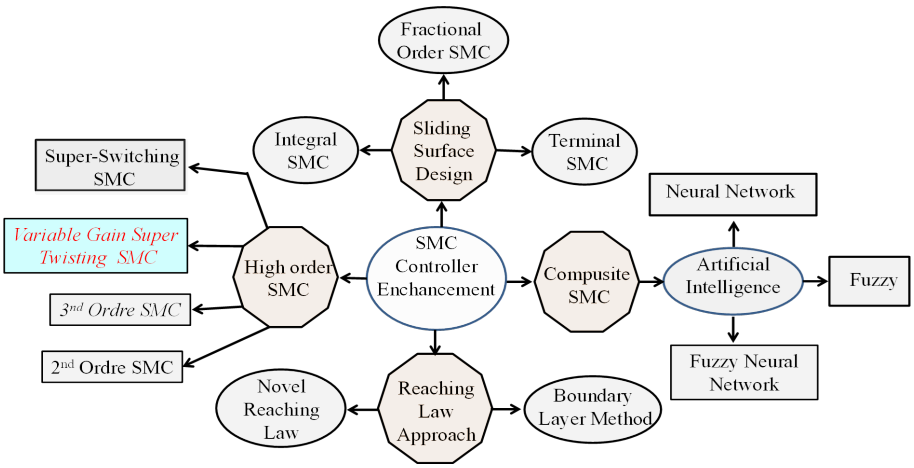

Fig. 2 Enhancement made in sliding mode control (SMC) [26]

high-quality power and current is proposed in [29], while minimizing steady-state error and reducing error and overshoot in reactive and active power.

In [30], the authors proposed a control strategy based on an amended formulation of the Super-Twisting Control with adaptive gains applied to a grid-connected wind power system based on DFIG. This method was compared with the conventional super-twisting control, and it was found that the proposed control technique reduces and facilitates control efforts through the development of a simplified sliding mode formulation, despite disturbances related to parameter variations and the randomness of wind speed. In [31], the authors explored adaptive second-order sliding mode control techniques to maximize the extracted wind energy in a WECS. Through modeling and simulation, it was demonstrated that the control method features robustness and relative simplicity.

To effectively address the chattering phenomenon and enhance the performance of the wind power system, a robust control strategy called the Variable-Gain Super-Twisting Algorithm (VGSTA) is proposed. The VGSTA strategy aims to reduce the chattering phenomenon, reduce response time (dynamic response), improve power quality (THD ≤ 5%), minimize overshoot, and effectively mitigate uncertainties and external disturbances. The performance and effectiveness of this control strategy are evaluated through the analysis of simulation results.

The main contributions of this paper are:

1. Improving the power quality delivered to the grid by proposing the robust controllers, in order to overcome the disadvantages of conventional controls in transient and steady-state conditions.
2. The proposed control method makes the wind power system perform very well in both wind speed sudden variation (random profile), and DFIG-electromechanical parameters change.
3. The VGSTA-SMC control minimizes overshoot, response time, and active/reactive power ripples, enhancing power quality and robustness against DFIG' parameters change.

This paper is organized as follows: firstly, the mathematical model of the Wind Turbine (WT) and Doubly Fed Induction Generator (DFIG) in the (d, q) reference frame is presented in Sections 2 and 3. In Section 4, the modeling of the fourth controls (FOC, C-SMC, 3O-SMC, and VGSTA-SMC) is discussed. Section 5 presents and discusses simulation results. Finally, the reported work is concluded.

2 Turbine modeling

The wind is a stochastic variable [32], characterized by its direction and speed, which are influenced by factors such as location and climate conditions [33]. The input power of a wind turbine is typically:

$$P_v = \frac{1}{2}\rho \cdot \pi \cdot R^2 \cdot V^3. \tag{1}$$

The wind turbine's mechanical power is expressed as follows:

$$P_t = P_v \cdot C_p = \frac{1}{2}\rho \cdot \pi \cdot R^2 \cdot v^3 \cdot C_p(\lambda, \beta), \tag{2}$$

where: R: radius of turbine (m), V: wind speed (m/s), λ: relative speed, ρ: air density ($\rho = 1.225$ kg m^3), $\beta°$: pitch angle (deg), Ω_t: turbine speed (rad/s), and C_p represents power coefficient can be described as:

$$C_p(\lambda, \beta) = n_1\left(\frac{n_2}{\lambda_i} - n_3\,\beta - n_4\right)e^{-\frac{n_5}{\lambda_i}} + n_6\lambda, \tag{3}$$

where:

$$\frac{1}{\lambda_i} = \frac{1}{\lambda + 0.08\beta} - \frac{0.035}{\beta^3 + 1},$$

$$\lambda = \frac{R \cdot \Omega_t}{V},$$

$n_1 = 0.5176$, $n_2 = 116$, $n_3 = 0.4$, $n_4 = 5$, $n_5 = 21$, $n_6 = 0.0068$.

The block diagram in Fig. 3 presents the model of the wind turbine.

The graph depicts the power coefficient (C_p) versus tip speed ratio (TSR or λ) for a pitch angle of 0° ($\beta = 0°$). The maximum value of C_p ($C_{p-\max} = 0.48$) is achieved when the blade pitch angle is set to 0° and the tip speed ratio is set to 8.1 (presents optimal λ_{opt}), as shown in Fig. 4.

Notably, this point corresponds to the maximum power point tracking (MPPT) condition [9]. By using poles placement method, the two PI controller adjustment gains (K_{P_MPPT} and K_{I_MPPT}) are given by [34]:

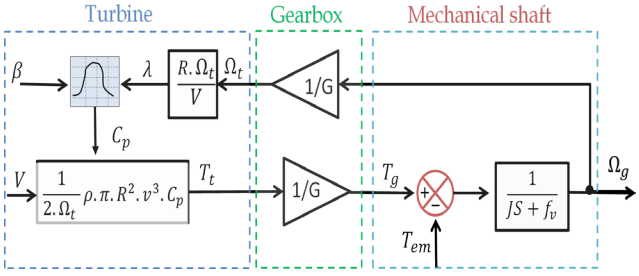

Fig. 3 Schematic block of wind turbine

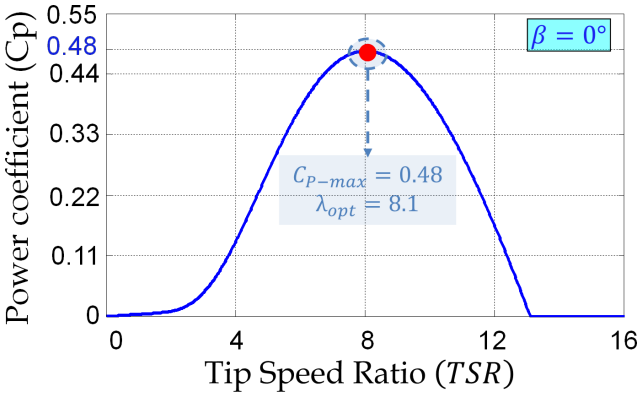

Fig. 4 Power coefficient C_p versus tip speed ratio (λ)

$$\begin{aligned} K_{I\_MPPT} &= \omega_n^2 J \\ K_{P\_MPPT} &= 2\ \xi\ J\ \omega_n - f_r \end{aligned}, \tag{4}$$

where: ω_n is the undamped natural frequency, ξ is the damping ratio, and for $\xi = 1$ and $\omega_n = 100$ rad/s, the values of K_{P_MPPT} and K_{I_MPPT} are given by:

$$\begin{aligned} K_{I\_MPPT} &= 10 \cdot 10^6 \\ K_{p\_MPPT} &= 2 \cdot 10^5 \end{aligned}. \tag{5}$$

Pitch angle control is a crucial aspect of wind turbine operation, primarily used to regulate the turbine's rotational speed and optimize power output. This control system often works in conjunction with MPPT algorithms to enhance energy capture (refer to Fig. 5). To achieve this, we employ a PI controller to keep the turbine operating near its maximum efficiency point, despite varying wind speeds [34–36]. Additionally, PI controllers are applied to pitch angle control to ensure the efficient and reliable operation of wind turbines.

3 Modeling of DFIG

After applying the Park transform, we obtain the rotor and stator voltages for the DFIG, additionally, the flux equations, as follows [10, 37, 38]:

$$\begin{cases} V_{sd} = R_s I_{sd} + d\Phi_{sd}/dt - \omega_s \Phi_{sq} \\ V_{rd} = R_r I_{rd} + d\Phi_{rd}/dt - (\omega_s - \omega_r)\Phi_{rq} \\ V_{sq} = R_s I_{sq} + d\Phi_{sq}/dt + \omega_s \Phi_{sd} \\ V_{rq} = R_r I_{rq} + d\Phi_{rq}/dt + (\omega_s - \omega_r)\Phi_{rd} \end{cases}, \tag{6}$$

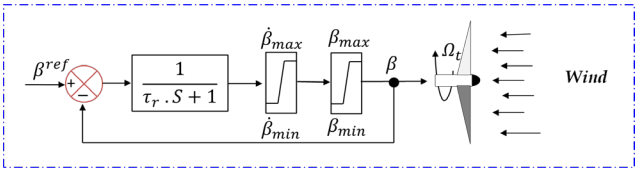

Fig. 5 Block diagram of the pitch angle β control

$$\begin{cases} \Phi_{sd} = L_s \cdot I_{sd} + M \cdot I_{rd} \\ \Phi_{rd} = L_r \cdot I_{rd} + M \cdot I_{sd} \\ \Phi_{sq} = L_s \cdot I_{sq} + M \cdot I_{rq} \\ \Phi_{rq} = L_r \cdot I_{rq} + M \cdot I_{sq} \end{cases}. \tag{7}$$

The electromagnetic torque:

$$\begin{cases} T_{em} = (3/2) \cdot \left[\dfrac{P \cdot M}{L_s} \left(\Phi_{sq} \cdot I_{rd} - \Phi_{sd} \cdot I_{rq} \right) \right] \\ T_{em} - T_r = J \dfrac{d\Omega_r}{dt} + f_r \Omega_r \end{cases}, \tag{8}$$

where: Ω_r is mechanical speed, T_r is the load torque, and J is total inertia.

The stator active and reactive powers:

$$\begin{cases} P_s = (3/2)\left[V_{sd} I_{sd} + V_{sq} I_{sq} \right] \\ Q_s = (3/2)\left[V_{sq} I_{sd} - V_{sd} I_{sq} \right] \end{cases}. \tag{9}$$

4 Control design

4.1 Field oriented control strategy

It is assumed that the stator voltage and the stator pulsation ω_s are constant, the electrical grid is stable, and the effect of stator resistances is negligible. This leads to a direct axis '*d*' alignment along the location of the stator flux vector with zero variation in the steady state [39]. Therefore, this can be expressed as follows:

$$\Phi_{sq} = 0, \ \Phi_{sd} = \Phi_s. \tag{10}$$

The DFIG model can be described on the previously written equation in the synchronous reference frame (refer to Fig. 6), where the direct axis "*d*" is aligned with the stator flux vector ($\Phi_{sd} = \Phi_s$), while the stator flux vector on the quadrature axis is non-existent ($\Phi_{sq} = 0$).

After neglecting the stator resistances, the following equations can be simplified:

$$V_{sd} = 0; \ V_{sq} = V_s = \omega_s \cdot \Phi_s, \tag{11}$$

$$\Phi_{sq} = L_s \cdot I_{sq} + M \cdot I_{rq} = 0, \tag{12}$$

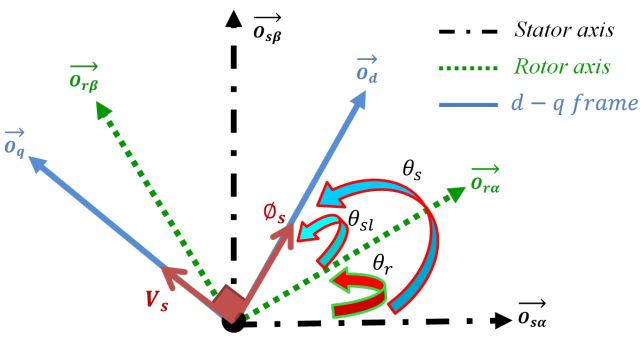

Fig. 6 Stator and rotor flux vectors along the *dq* frame

$$I_{sq} = -\left[M \cdot I_{rq} / L_s\right], \tag{13}$$

$$\begin{aligned} P_s &= -(3/2)\cdot\left[\frac{M}{L_s} V_s \cdot I_{rq}\right] \\ Q_s &= (3/2)\cdot\left[\left(\frac{V_s^2}{L_s \cdot \omega_s} - \frac{M \cdot V_s}{L_s} I_{rd}\right)\right] \end{aligned}. \tag{14}$$

The electromagnetic torque:

$$T_{em} = -P \cdot \left[\frac{3 \cdot M \cdot \Phi_s}{2 \cdot L_s}\right] \cdot I_{rq}. \tag{15}$$

To control the DFIG, expressions show the relationship between the currents and the rotor voltages applied to it.

$$\begin{cases} V_{sd-PI} = R_s I_{sd} + d\Phi_{sd} / dt - \omega_s \Phi_{sq} = 0 \\ V_{sq-pi} = R_s I_{sq} + d\Phi_{sq} / dt + \omega_s \Phi_{sd} = \omega_s \Phi_s \\ V_{rd-PI} = R_r I_{rd} + \sigma \cdot dI_{rd} / dt - (\omega_s - \omega_r) \cdot \sigma \cdot I_{rq} \\ V_{rq-PI} = R_r I_{rq} + \sigma \cdot dI_{rq} / dt + (\omega_s - \omega_r) \\ \sigma \cdot I_{rd} + (\omega_s - \omega_r) \dfrac{M^2}{L_s} \Phi_s \end{cases}. \tag{16}$$

The schematic diagram of the field-oriented control based PI, a simple yet effective control strategy widely employed in industrial applications [34], is illustrated in Fig. 7.

The PI controller has two parameters: the proportional gain (K_{P_PI}) and the integral gain (K_{I_PI}). The K_{P_PI} gain determines how quickly the controller responds to errors, while the K_{I_PI} gain determines how well the controller eliminates steady-state errors. The calculation of PI controller gains depends on the system's parameters [34, 40, 41]. The open-loop transfer function (OLTF) incorporating the controllers is expressed as follows (taking into account that the variable '*s*' represents the Laplace variable):

$$\text{OLTF} = \frac{\text{output}}{\text{input}} = \frac{S + \dfrac{K_{I\_PI}}{K_{P\_PI}}}{\dfrac{S}{K_{P\_PI}}} \frac{\dfrac{V_s L_m}{L_s\left(L_r - \dfrac{L_m^2}{L_s}\right)}}{S + \dfrac{R_r L_s}{L_s\left(L_r - \dfrac{L_m^2}{L_s}\right)}}. \tag{17}$$

To eliminate the zero present in the transfer function, we choose the method of pole compensation for the regulator synthesis:

$$\frac{K_{I\_PI}}{K_{P\_PI}} = \frac{R_r L_s}{L_s\left(L_r - \dfrac{L_m^2}{L_s}\right)}, \tag{18}$$

$$\text{OLTF} = \frac{K_{P\_PI} \dfrac{V_s L_m}{L_s\left(L_r - \dfrac{L_m^2}{L_s}\right)}}{S}. \tag{19}$$

For a response time t_r (5%) = 1 ms, we obtain:

$$\begin{aligned} K_{P\_PI} &= \frac{1}{10^{-3}} \frac{L_s L_r L_m^2}{V_s L_m} = 7.57491 \cdot 10^{-4} \\ K_{I\_PI} &= \frac{1}{10^{-3}} \frac{L_s R_r}{V_s L_m} = 53.5455 \cdot 10^{-2} \end{aligned}. \tag{20}$$

4.2 Design of conventional SMC

For many years, researchers have continuously proposed various control strategies for DFIG, among which SMC stands out as a nonlinear and robust method [42]. It offers several advantages, including a simple and easily implementable structure. Furthermore, it enables effective control even in the presence of disturbances and uncertainties, with its design grounded in three main elements [43–46].

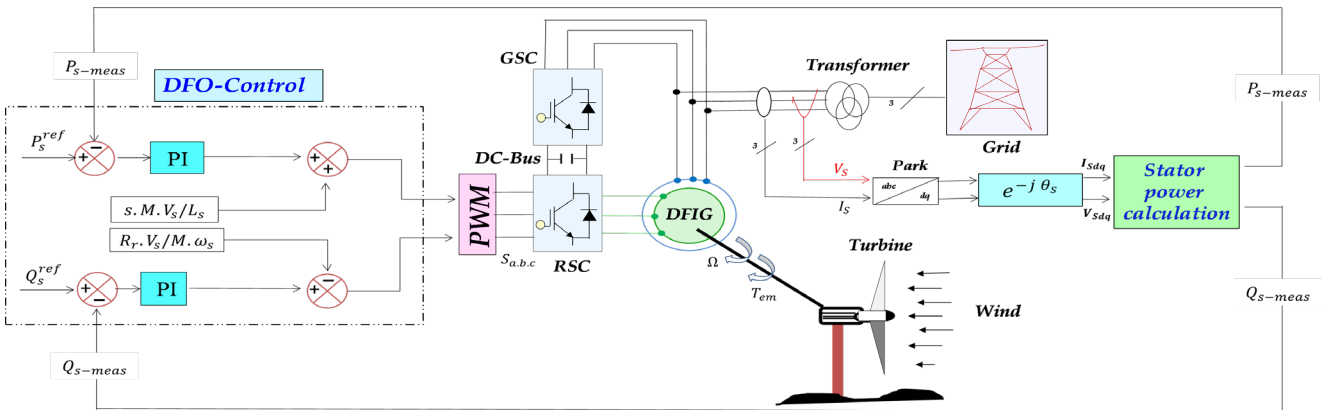

Fig. 7 Schematic diagram of DFIG-field oriented control based on PI controllers

4.2.1 Identification of the sliding surface

The choice of sliding surface is expressed by:

$$\begin{cases} e_P = P_s^{ref} - P_s \\ e_Q = Q_s^{ref} - Q_s \end{cases}, \quad \begin{cases} \dot{e}_P = \dot{P}_s^{ref} - \dot{P}_s \\ \dot{e}_Q = \dot{Q}_s^{ref} - \dot{Q}_s \end{cases}. \tag{21}$$

By substituting the derivatives of active and reactive powers into Eq. (22), we obtain:

$$\begin{cases} \dot{e}_P = \dot{P}_s^{ref} + \left(3MV_s/2L_s\right)\left[-\dfrac{R_r}{\sigma L_r} I_{rd} + s\omega_s I_{rq} + \dfrac{V_{rq}}{\sigma L_r}\right] \\ \dot{e}_Q = \dot{Q}_s^{ref} + \left(3MV_s/2L_s\right)\left[-s\omega_s I_{rd} - \dfrac{R_r}{L_r\sigma} I_{rq} \right. \\ \qquad\qquad \left. -\dfrac{sMV_s}{L_s L_r \sigma} + \dfrac{V_{rd}}{\sigma L_r}\right] \end{cases}, \tag{22}$$

with: σ is the dispersion coefficient between windings d and q, usually is: $\sigma = 1 - (M^2/L_s L_r)$.

4.2.2 The convergence condition

The stability condition is given by:

$$e_P \cdot \dot{e}_P \le 0, \;\; e_Q \cdot \dot{e}_Q \le 0. \tag{23}$$

4.2.3 The convergence condition

We substituting V_{rq} by $\underbrace{\left[-r_1 \cdot \text{sign}\left(e_P\right) + V_{rq\_eq}\right]}_{V_{rq\_n}}$ and V_{rd} by $\underbrace{\left[-r_2 \cdot \text{sign}\left(e_Q\right) + V_{rd\_eq}\right]}_{V_{rd\_n}}$ in Eq. (19), becomes:

$$\begin{aligned} V_{rq\_eq} &= -\left[2 \cdot \sigma \cdot L_s \cdot L_r / 3 \cdot V_s \cdot M\right] P_s^{ref} - \sigma \cdot L_r \cdot Y_2 \\ V_{rd\_eq} &= -\left[2 \cdot \sigma \cdot L_s \cdot L_r / 3 \cdot V_s \cdot M\right] Q_s^{ref} - \sigma \cdot L_r \cdot Y_1 \end{aligned}. \tag{24}$$

The C-SMC controller gains can be determined by the following expressions [47]:

$$\begin{aligned} r_1 + r_2 &= 2\xi\omega_n \\ r_1 r_2 &= \omega_n^2 \end{aligned}. \tag{25}$$

To ensure stability of the considered system, gains r_1 and r_2 must be constant and positive (refer to Table 1). Based on the Eq. (24), we can construct the scheme for C-SMC as illustrated in Fig. 8.

4.3 Design of third order SMC

The third-order sliding mode controller (3O-SMC) is a robust control strategy that has been proven effective in controlling systems. It is considered an alternative to both nonlinear and linear strategies, overcoming the main disadvantages of conventional SMC technology described in the literature. This technology is based on the Super Twisting algorithm, and the 3O-SMC control can be expressed using the following equations [48]:

$$V(t) = \gamma_1(t) + \gamma_2(t) + \gamma_3(t), \tag{26}$$

where: $V(t)$: Output of the proposed 3O-SMC method:

$$\begin{cases} \gamma_1(t) = \partial_1 |e|^{0.5} \cdot \text{sign}(e) \\ \gamma_2(t) = \partial_2 \int \text{sign}(e)\, dt \\ \gamma_3(t) = \partial_3 \, \text{sign}(e) \end{cases}. \tag{27}$$

Offset, $\gamma_1(t)$, $\gamma_2(t)$ and $\gamma_3(t)$ in the Eq. (28), we get:

$$V(t) = \partial_1 |e|^{0.5} \cdot \text{sign}(e) + \partial_2 \int \text{sign}(e)\, dt + \partial_3 \text{sign}(e). \tag{28}$$

Table 1 Gains values of diffrent controllers

Strategies:	PI	C-SMC	3O-SMC	VGSTA-SMC
Parameters	$K_{P\_PI} = 7.575 \cdot 10^{-4}$	$r_1 = 80$	$\partial_1 = 0.5$	$\alpha_1 = 11$
			$\partial_2 = 9900$	$\alpha_2 = 9900$
	$K_{I\_PI} = 53.54 \cdot 10^{-2}$	$r_2 = 900$	$\partial_3 = 10$	$\alpha_3 = 0.6$

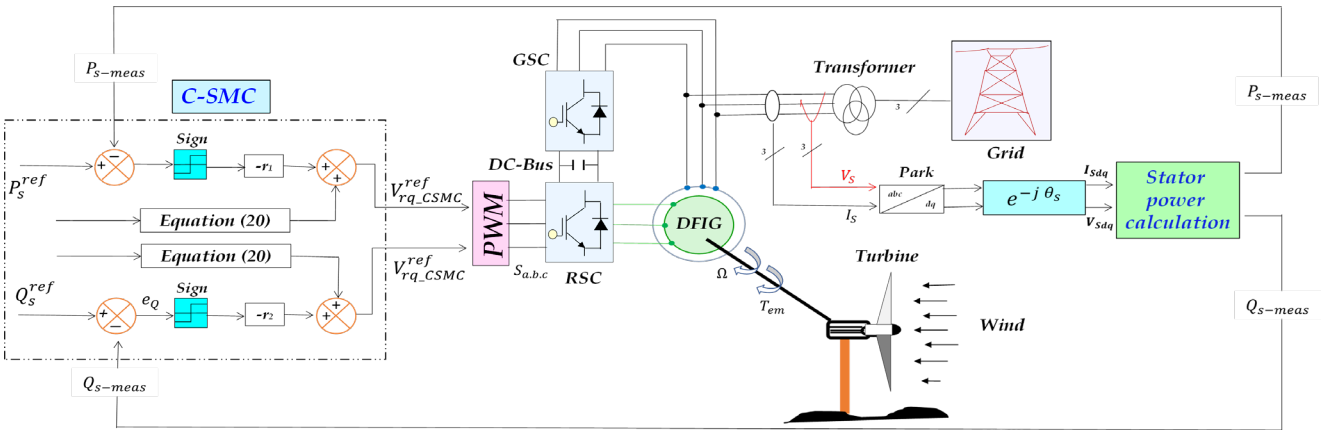

Fig. 8 Schematic diagram of conventional SMC algorithm based on DFIG

The sliding surfaces shown in Eq. (21) are used as inputs for the 3O-SMC control law. Thus, based on the last Eq. (28) obtained, we can express $V_{rd\_3O\text{-}SMC}^{ref}$ and $V_{rq\_3O\text{-}SMC}^{ref}$ as follows:

$$\begin{cases} V_{rd\_3O\text{-}SMC}^{ref} = \partial_1 \left|e_Q\right|^{0.5} \operatorname{sign}\left(e_Q\right) \\ \qquad\qquad +\partial_2 \int \operatorname{sign}\left(e_Q\right) dt + \partial_3 \operatorname{sign}\left(e_Q\right) \\ V_{rq\_3O\text{-}SMC}^{ref} = \partial_1 \left|e_P\right|^{0.5} \operatorname{sign}\left(e_P\right) \\ \qquad\qquad +\partial_2 \int \operatorname{sign}\left(e_P\right) dt + \partial_3 \operatorname{sign}\left(e_P\right) \end{cases}. \tag{29}$$

The tuning constants ∂_1, ∂_2, and ∂_3 are used to improve the performance of the 3O-SMC method. These gains are calculated using mathematical formulas and further refined through manual adjustments until the desired result is achieved (Table 1). The 3O-SMC controller scheme is presented in Fig. 9.

4.4 Design of VGSTA-SMC

The Variable Gain Super Twisting Algorithm (VGSTA) can be expressed as follows:

$$V_{\text{VGSTA}} = -\alpha_1(t,x)\cdot W_1(S) - \int_0^t \alpha_2(t,x)\cdot W_2(e)\,dt, \tag{30}$$

where:

$$\begin{cases} W_1(e) = |e|^{0.5} \operatorname{sign}(e) + \alpha_3 e \\ W_2(e) = \dfrac{1}{2}\operatorname{sign}(e) + \dfrac{3}{2}\alpha_3 |e|^{0.5} \operatorname{sign}(e) + \alpha_3^2 e \end{cases}. \tag{31}$$

The standard Super Twisting Algorithm (STA) can be restored when $\alpha_3 = 0$ and the gains α_1 and α_2 are kept constant and unchanged. However, by setting $\alpha_3 > 0$, the VGSTA-SM control allows for dealing with perturbations that grow outside the sliding surface.

Additionally, the variable gains α_1 and α_2 make the sliding surface insensitive to perturbations. It should be noted that the control variable is continuously smooth, in contrast to the discontinuous nature of the Conventional Sliding Mode Control (C-SMC) [27, 48].

The uncertainty and perturbation supported by VGSTA can be expressed as follows:

$$\begin{aligned} \tilde{\varepsilon}(h_1,\ e+\alpha\ h_1,t) &= \underbrace{-\tilde{\varepsilon}(h_1,\ \alpha\ h_1,t)}_{g_2(h_1,t)} \\ &+ \underbrace{\tilde{\varepsilon}(h_1,\ e+\alpha\ h_1,t) - \tilde{\varepsilon}(h_1,\ \alpha\ h_1,t)}_{g_1(h_1,e,t)}, \end{aligned} \tag{32}$$

where:

$$\begin{aligned} &\left|g_1(h_1,\ e,\ t)\right| \le \vartheta_1(t,x)\left|W_1(e)\right| \ \text{ with } \vartheta_1(t,x) \ge 0 \\ &\left|\frac{d}{dt} g_2(h_1,t)\right| \le \vartheta_2(t,x)\left|W_2(e)\right| \ \text{ with } \vartheta_2(t,x) \ge 0 \end{aligned}. \tag{33}$$

$\vartheta_2(t, x)$ and $\vartheta_1(t, x)$, are known continuous functions.

System driven by the VGSTA (Eq. (30)) can be expressed as:

$$\begin{aligned} \dot{h}_1 &= (A_{11} + A_{12}\alpha)h_1 + A_{12}e \\ \dot{e} &= -\alpha_1(t,x)W_1(e) + h + g_1(h_1,\ e,\ t) \\ \dot{h}_0 &= -\alpha_2(t,x)W_2(e) + \frac{d}{dt} g_2(h_1,t) \end{aligned}. \tag{34}$$

Theorem 1. Suppose that for some known continuous functions $\vartheta_1(t, x) \ge 0$, $\vartheta_2(t, x) \ge 0$ the inequalities of Eq. (30) are satisfied. Then for any initial condition ($h_1(0)$, $e(0)$, $h_0(0)$) the sliding surface $e = 0$, will be reached in finite time if the variable gains are selected as [29]:

$$\begin{aligned} \alpha_1(t,x) &= \delta + \frac{1}{\beta}\left(\begin{array}{l} \dfrac{1}{4\aleph}\left(2\aleph\vartheta_1 + \vartheta_2\right)^2 + 2\aleph\vartheta_2 + \aleph \\ +\left(2\aleph + \vartheta_1\right)\left(\beta + 4\aleph^2\right) \end{array}\right), \\ \alpha_2(t,x) &= \beta + 4\aleph^2 + 2\aleph h_1(t,x) \end{aligned} \tag{35}$$

where $\beta > 0$, $\aleph > 0$, $\delta > 0$, are arbitrary positive constants. The time it takes to reach the sliding surface can be estimated by:

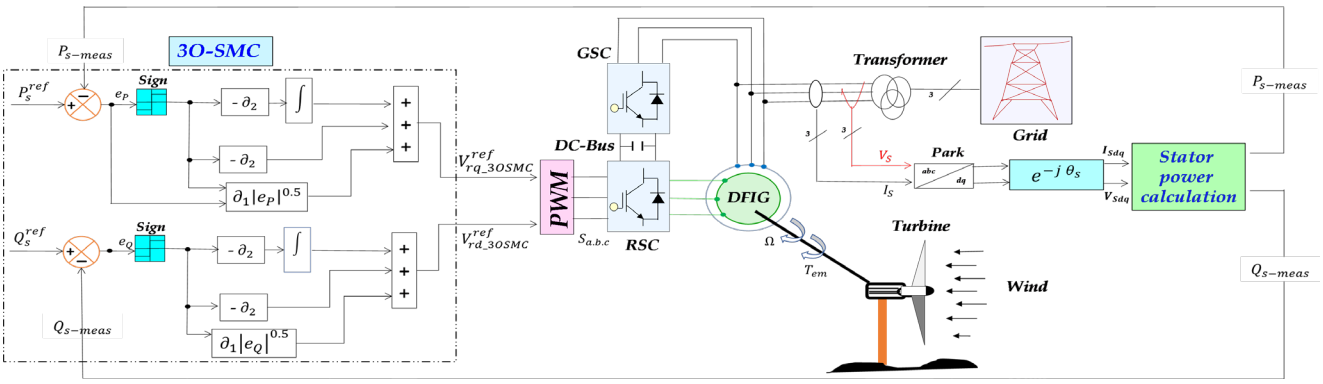

Fig. 9 Schematic diagram of third order SMC algorithm based on DFIG

$$T=\frac{2}{\gamma_2}\ln\left(\frac{\gamma_2}{\gamma_1}V^{0.5}\left(e(0),\ h_0(0)\right)+1\right), \tag{36}$$

where $V(e,\ h_0)=\xi^T P\xi$, with $\xi^T=\left[|e|^{0.5}\operatorname{sign}(e)+\alpha_3 e,\ h_0\right]$ and $\gamma_1=\aleph\lambda_{\min}^{0.5}\{P\}/\lambda_{\max}\{P\},\ \gamma_2=2\aleph\alpha_3/\lambda_{\max}\{P\}$.

Proof. The quadratic form:

$$V\left(e,\ h_0\right)=\xi^T P\xi, \tag{37}$$

where:

$$\xi^T=\left[|e|^{0.5}\operatorname{sign}(e)+\alpha_3 e,\ h_0\right], \tag{38}$$

$$P=\begin{bmatrix}P_1 & P_3\\ P_3 & P_2\end{bmatrix}=\begin{bmatrix}\beta+4\aleph^2 & -2\aleph\\ -2\aleph & 1\end{bmatrix}. \tag{39}$$

For arbitrary positive constants $\beta>0,\ \aleph>0$ the function is a Lyapunov function for the subsystem $(e,\ h_0)$ of Eq. (34), demonstrating finite-time convergence. Equation (37) is positive definite, continuously everywhere, and differentiable everywhere except on the set $S=\left\{(e,\ h_0)\in R^2\,|\,e=0\right\}$. The inequalities of Eq. (33) can be expressed as $g_1(h_1,e,t)=\propto_1(t,x)W_1(e)$ and $d/dt\,g_2(h_1,t)=\propto_2(t,x)W_2(e)$ for some functions $|\propto_1(t,x)|\le\vartheta_1(t,x)$ and $|\propto_2(t,x)|\le\vartheta_2(t,x)$. Utilizing these functions and recognizing that:

$$\begin{aligned}\dot{\xi}&=\begin{bmatrix}W_1'(e)\left\{-\alpha_1(t,x)W_1(e)+h_0+g_1(x,t)\right\}\\ -\alpha_2(t,x)W_2(e)+\dfrac{d}{dt}g_2(x,t)\end{bmatrix}\\ &=W_1'(e)\begin{bmatrix}-\left(\alpha_1(t,x)-\propto_1(t,x)\right) & 1\\ -\left(\alpha_2(t,x)-\propto_2(t,x)\right) & 0\end{bmatrix}.\end{aligned} \tag{40}$$

At every point in $R^2\setminus S$ setminus S, where this derivative exists. Similarly, one can calculate the derivative of $V(x)$ on the same set as:

$$\begin{aligned}\dot{V}(e,h_0)&=W_1'(e)\xi^T\left(A^T(t,x)P+P\,A(t,x)\right)\xi\\ &=-W_1'(e)\xi^T Q(t,x)\xi,\end{aligned} \tag{41}$$

where:

$$Q(t,x)=\begin{bmatrix}2\left(\alpha_1(t,x)-\propto_1\right)P_1+2\left(\alpha_2(t,x)-\propto_2\right)P_3 & *\\ \left(\alpha_1(t,x)-\propto_1\right)P_3+\left(\alpha_2(t,x)-\propto_2\right)P_2-P_1 & -2P_3\end{bmatrix}. \tag{42}$$

Choosing P as specified in Eq. (38) and the gains according to Eq. (37), we obtain:

$$\begin{aligned}&Q-2\aleph I\\ &=\begin{bmatrix}2\beta\alpha_1+4\aleph\left(2\aleph\alpha_1-\alpha_2\right) & *\\ -2\left(\beta+4\aleph^2\right)\propto_1+4\aleph\propto_2-2\aleph & \\ \alpha_2-2\aleph\alpha_1-\left(\beta+4\aleph^2\right)+2\aleph\propto_1-\propto_2 & -2P_3\end{bmatrix},\\ &Q-2\aleph I\\ &=\begin{bmatrix}2\beta\alpha_1-\left(\beta+4\aleph^2\right)\left(4\aleph+2\propto_1\right)+\ 4\aleph\propto_2-2\aleph & *\\ 2\aleph\propto_1-\propto_2 & 2\aleph\end{bmatrix},\end{aligned}$$

That is positive definite for every value of $(t,\ x)$. This indicates that:

$$\begin{aligned}\dot{V}&=-W_1'(e)\xi^T Q(t,x)\xi\le-2\aleph W_1'(e)\xi^T\xi\\ &=-2\aleph\left(\frac{1}{2|e|^{0.5}}+\alpha_3\right)\xi^T\xi.\end{aligned} \tag{43}$$

Since, $\lambda_{\min}\{P\}\|\xi\|_2^2\le\xi^T P\xi\le\lambda_{\max}\{P\}\|\xi\|_2^2$ where:

$$\|\xi\|_2^2=\xi_1^2+\xi_2^2=|e|+2\alpha_3|e|^{\frac{3}{2}}+\alpha_3^2e^2+h_0^2, \tag{44}$$

is the Euclidean norm of ξ, and:

$$|\xi_1|\le\|\xi\|_2\le\frac{V^{0.5}\left(e,\ h_0\right)}{\lambda_{\min}^{0.5}\{P\}}, \tag{45}$$

we can conclude that:

$$\dot{V}\le-\gamma_1V^{0.5}\left(e,\ h_0\right)-\gamma_2V\left(e,\ h_0\right). \tag{46}$$

Note that the trajectories cannot stay on the set: $S=\left\{(e,\ h_0)\in R^2\,|\,e=0\right\}$. This means that V is a continuously decreasing function and we can conclude that the equilibrium point $(e,\ h_0)=0$ is reached in finite time from every initial condition. Since the solution of the differential equation:

$$\dot{V}=-\gamma_1V^{0.5}-\gamma_2V,\ V\left(0\right)\ge0, \tag{47}$$

is given by:

$$V\left(t\right)=\exp\left(-\gamma_2t\right)\left[V\left(0\right)^{0.5}+\frac{\gamma_1}{\gamma_2}\left(1-\exp\left(\frac{\gamma_2}{2}t\right)\right)\right]^2. \tag{48}$$

It follows that $(e(t),\ h_0(t))$ converges to zero in finite time and reaches that value at most after a time given by Eq. (37). This concludes the proof of ***Theorem 1***.

When $P(x)=const$, p first SMC can handle bounded perturbations $\xi(x(t),\ t)$ that are measurable along system

trajectories. Conversely, the STA with constant gains α_1 and α_2 can compensate for Lipschitz continuous perturbations $\xi(x, t)$ along system trajectories, where their absolute value cannot increase faster than a linear function of t or faster than linearly with respect to $|e(t)|^{0.5}$ along the system trajectories.

Based on Eq. (30), can be expressed the equations $V_{rd\_\mathrm{VGSTA}}^{ref}$, and $V_{rq\_\mathrm{VGSTA}}^{ref}$ as follows:

$$\begin{cases} V_{rd\_\mathrm{VGSTA}}^{ref} = -\alpha_1 \cdot \left[|e_Q|^{0.5} \operatorname{sign}(e_Q) + \alpha_3 e_Q \right] \\ -\int_0^t \left(\alpha_2 \cdot \left[\frac{1}{2} \operatorname{sign}(e_Q) + \frac{3}{2} \alpha_3 \cdot |e_Q|^{0.5} \operatorname{sign}(e_Q) \alpha_3^2 \cdot e_Q \right] \right) dt \\ V_{rq\_\mathrm{VGSTA}}^{ref} = -\alpha_1 \cdot \left[|e_P|^{0.5} \operatorname{sign}(e_P) + \alpha_3 e_P \right] \\ -\int_0^t \left(\alpha_2 \cdot \left[\frac{1}{2} \operatorname{sign}(e_P) + \frac{3}{2} \alpha_3 \cdot |e_P|^{0.5} \operatorname{sign}(e_P) \alpha_3^2 \cdot e_P \right] \right) dt \end{cases} . \tag{49}$$

The values of the constants , and , which are calculated using Eq. (35), are presented in Table 1. From the last two equations, we can construct the scheme of the VGSTA-SMC controller as illustrated in Fig. 10.

5 Analysis of performance indices

The controller's performance is evaluated using four criteria: Integral of Absolute Error (IAE), Integral Time Absolute Error (ITAE), Integral of Squared Error (ISE), and Integral Time Square Error (ITSE). These metrics provide a quantitative evaluation of the controller's performance [38, 46]:

$$\mathrm{IAE} = \int_0^t \lfloor e(t) \rfloor dt, \tag{50}$$

$$\mathrm{ITAE} = \int_0^t t \cdot \lfloor e(t) \rfloor dt, \tag{51}$$

$$\mathrm{ISE} = \int_0^t e^2(t) dt, \tag{52}$$

$$\mathrm{ITSE} = \int_0^t t \cdot e^2(t) dt. \tag{53}$$

6 Simulation results

In this paper, a 1.5 MW DFIG is connected to a 398/690V grid with rated parameters are given in Table A1. Additionally, the wind-turbine parameters are given in Table A2, are also considered, Table 1 presents respectively the parameters used in the PI, 3O-SMC, and VGSTA-SMC controllers. Notably, the parameters used for active power control are the same as those used for reactive power control. The following teste will be conducted using MATLAB/Simulink® environment:

- *Test-1*: Electromechanical wind turbine-DFIG parameters.
- *Test-2*: Decoupling terms.
- *Test-3*: Reference tracking.
- *Test-4*: Evaluating Control Strategies using Phase-Plane Trajectories
- *Test-5*: Robustness tests and performance comparison.

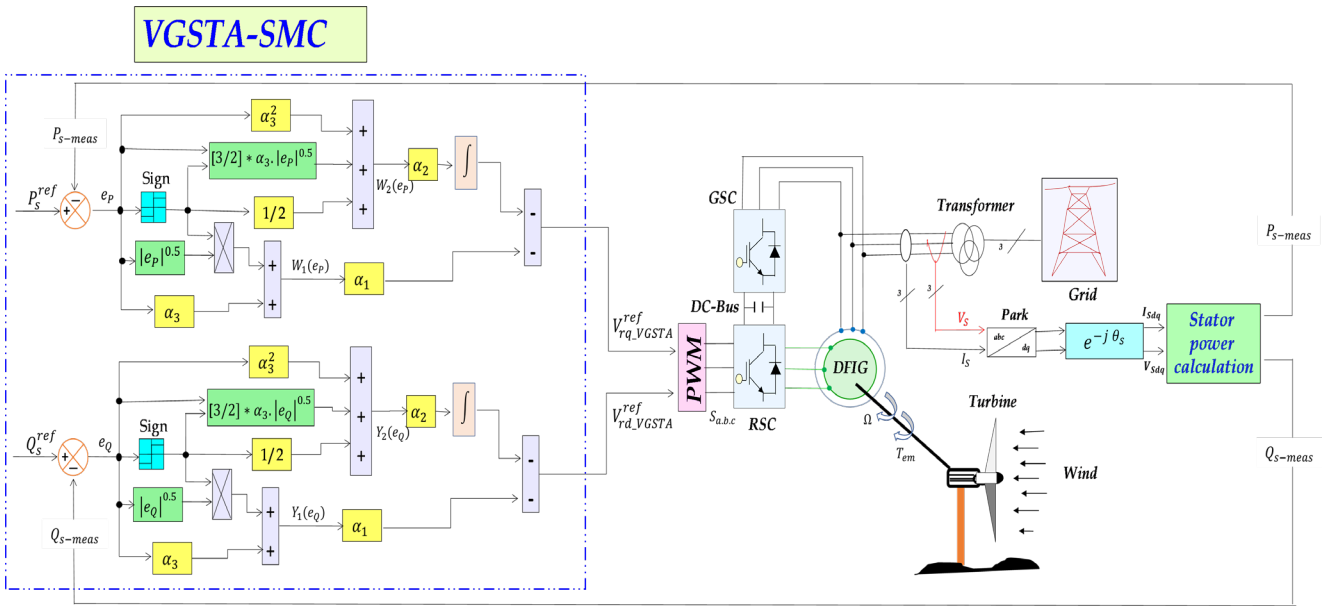

Fig. 10 Schematic diagram of variable gain super twisting algorithm SMC algorithm based on DFIG

6.1 Electromechanical wind turbine-DFIG parameters

The simulation test serves the purpose of thoroughly evaluating the performance of conventional control strategies within a wind turbine system, particularly under variable wind conditions. The objective is to gain comprehensive insights into various crucial parameters. The wind speed analysis focuses on understanding the system's response to changes in wind conditions, ensuring its adaptability and operational effectiveness.

Rotation speed examination provides a critical assessment of the turbine's ability to maintain optimal rotational speeds amidst fluctuating winds.

The evaluation of slip is pivotal for gauging the efficiency of the wind turbine in harnessing power from the wind. The scrutiny of rotor currents sheds light on the electrical behavior and control of the rotating components, while the assessment of rotor power delves into the efficiency of power conversion. The analysis of stator active power further illuminates the electrical power output, while stator currents examination offers insights into the electrical behavior and control of stationary components. Revisiting rotor currents underscores their dynamic significance in comprehending the wind turbine's response.

Fig. 11 showcases the simulation results of a wind turbine generator employing conventional control under a random wind speed profile, with a peak of 12 m/s. Notably, the generator exhibits both sub-synchronous (below 1500 rpm) and super-synchronous (above 1500 rpm) modes while maintaining zero reactive power (Q_s = 0 Var). The MPPT strategy dictates the target stator active power (P_{s-ref}), visualized in (f) closely following its reference.

Slip behavior (s), shown in (c), is carefully confined within a stable zone between 0.24 and −0.22. This ensures efficient operation, as positive slip (>0) signifies decreased efficiency due to generator speed falling below synchronous, while negative slip (<0) indicates potential rotor power increase due to exceeding synchronous speed.

Notably, mechanical speed (N_r) reaches 1500 rpm at 0.4S, 1.12 sec, 1.69 sec, and 1.79 sec within the stable zone highlighting efficient rotor power generation, this can be expressed mathematically $P_r = -s \cdot P_s$ (refer Table 2). Rotor currents (I_{r-abc}), depicted in (d), display sinusoidal waveforms with slight ripples influenced by slip changes. They remain manageable within the stable zone but may increase with extreme slip values, reflecting generator adjustments to high or low speeds. In contrast, stator currents (I_{s-abc}) in (h) maintain a stable sinusoidal shape unaffected by slip due to their distinct generation source. Finally, Fig. 11(e) exhibits a power factor very close to unity $\left(PF = P_s \Big/ \sqrt{P_s^2 + Q_s^2} \approx 1\right)$ thanks to the zero-reference reactive power, emphasizing efficient real power exchange with the grid and accurate MPPT tracking. Based on the simulation results, we can create Table 3, which illustrates the electromechanical values in the steady state.

6.2 Decoupling terms

This test aims to confirm the efficacy of the proposed control algorithm effectively separates the direct (d) and quadrature (q) axes compared to conventional controllers (PI, C-SMC, and 3O-SMC). Successful decoupling ensures that alterations or disturbances in one axis do not influence the other, thereby contributing to improved controllability and stability of the system. Fig. 12 illustrates the simulation results of the decoupling terms test for both conventional and proposed control methods, the reference active and reactive power profiles can be found in Table 4.

The simulation results obtained in Fig. 12 (to the left) of the term decoupling test highlight the effectiveness of the proposed control algorithm (VGSTA-SMC) in separating the d–q axis components, especially when compared to conventional controllers (PI, C-SMC, and 3O-SMC). Successful decoupling is apparent as alterations or disturbances in one axis do not significantly impact the other, contributing to an improved level of controllability and stability within the system. This is evidenced by the notable reduction in cross-coupling (Overshoot ≈ 2%) in the proposed control, reaching an almost negligible level. Such a reduction indicates that one axis has minimal influence on the other, thereby enhancing the control capability and overall system stability. Fig. 12 (to the right) displays the Total Harmonic Distortion (THD) values obtained using different controller strategies: PI, C-SMC, 3O-SMC, and VGSTA-SMC.

The Fast Fourier Transform (FFT) method is employed to calculate the THD values.

The THD Is-abc rates for the PI controller, conventional sliding mode control (C-SMC), and VGSTA are shown to be 14.05%, 3.81%, and 3.62%, respectively, all below the 5% acceptable limit for most power systems. The elevated THD value in the PI controller is attributed to the presence of the chattering phenomenon, which can introduce significant harmonic distortion in the system. Therefore, based on the THD analysis, VGSTA-SMC can be considered a favorable choice among the controllers (C-SMC and 3O-SMC).

Furthermore, the analysis of active and reactive power errors reveals that the VGSTA-SMC controller has the lowest errors (+/− 1.5469), making it the most effective controller for tracking the desired active and reactive power

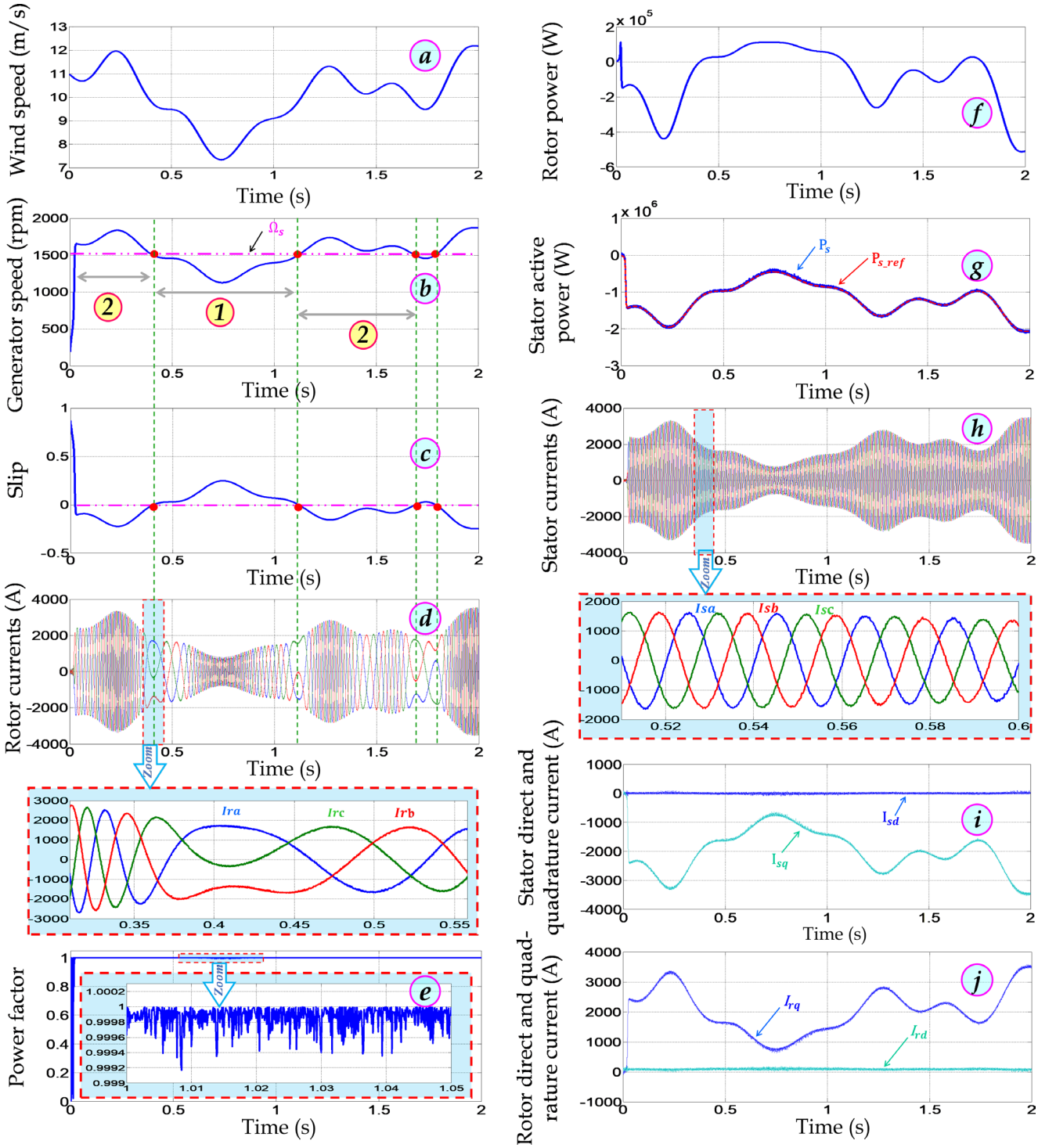

Fig. 11 Simulation results of DFIG parameter under three operating

Table 2 Rotor power flow performance

Modes	f_s (Hz)	f_r (Hz)	P_s (Mw)	P_r (W)	S	N_r (rpm)
Synchronous	50	0	$-1.06 \cdot 10^{+6}$	0	0	1500
Sub-synchronous	50	+11	$-5.006 \cdot 10^{+5}$	$-1.111 \cdot 10^{+5}$	0.2219	1167
Super-synchronous	50	−10.5	$-1.882 \cdot 10^{+6}$	$-3.990 \cdot 10^{+5}$	−0.212	1818

controller for tracking the desired active and reactive power. In comparison, the 3O-SMC controller exhibits errors of +/− 3.0805, followed by the C-SMC controller with errors of +/− 31.235, and the PI controller with the highest errors of +/− 50.510. These results are succinctly summarized in Table 5, providing a comprehensive overview of the

Table 3 Wind turbine electromechanical values for steady state

Parameters	Maximum value	Minimum value
Wind speed v (m/s)	12.18	7.3
Rotation speed n (rpm)	1872	1129
Rotor current I_r (A)	3563	−3565
Slip S (–)	0.24	−0.22
Rotor power P_r (W)	1.12 · 105	−5.13 · 105
Stator active power P_s (MW)	−2.08	−0.436
Stator current I_s (A)	3500	−3492
Rotor direct current I_{rd} (A)	85.5	85.5
Rotor quadrature current I_{rq} (A)	716	3516
Stator direct current I_{sd} (A)	0	0
Stator quadrature current I_{sq} (A)	−3454	−7313
Power factor P_F (–)	0.99	1

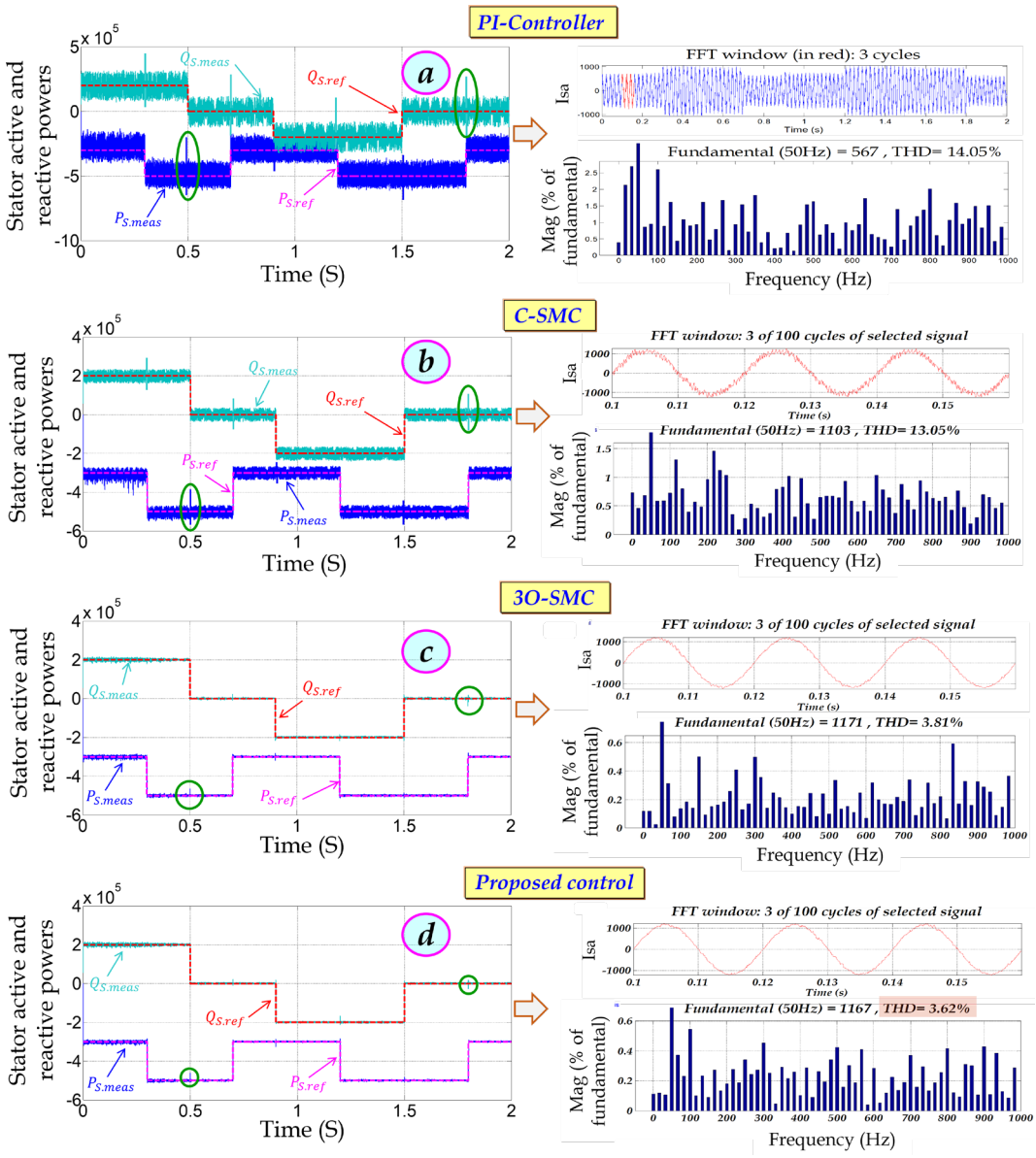

Fig. 12 Simulation results of decoupled terms and power quality for conventional and proposed controls

Table 4 Active and reactive power reference profiles for decoupling terms test

Time (s)	Stator active power P_s (MW)	Stator reactive power Q_s (MVar)
[0–0.3]	−0.3	+0.2
[0.3–0.5]	−0.5	+0.2
[0.5–0.7]	−0.5	0
[0.7–0.9]	−0.3	0
[0.9–1.2]	−0.3	−0.2
[1.2–1.5]	−0.5	−0.2
[1.5–1.8]	−0.5	0
[1.8–2]	−0.3	0

Table 5 Recapitulation results for PI, C-SMC, 3O-SMC, and VGSTA-SMC

Control	THD I_{s-abc} (%)	THD I_{r-abc} (%)	Overshoot (%)	Response time (ms)	Power Error (KW/KVar)
PI	14.05	223.57	Remarquable (≈70%)	1.7	+/− 50.510
C-SMC	13.03	207.14	Remarquable (≈60%)	1.2	+/− 31.235
3O-SMC	3.81	89.73	Neglected (≈5%)	0.5	+/− 3.0805
VGSTA-SMC	3.62	91.46	Neglected (≈2%)	0.3	+/− 1.5469

controllers' performance in terms of decoupling, harmonic distortion, response time, and power tracking capability.

6.3 Reference tracking

The main objective of this test is to evaluate and compare the performance of different control strategies in tracking the reference power under varying conditions. Specifically, the tests aim to assess the tracking accuracy of each control strategy, including PI, C-SMC, 3O-SMC, and VGSTA-SMC, under different scenarios. In Case I, the reference active power is generated by the MPPT strategy, and in Case II, the reference active power is a step change. In both cases, the reactive power reference is kept at zero to ensure a unit power factor ($F_P = 1$) on the stator side of the DFIG.

The results in Fig. 13 indicate that, the VGSTA-SMC strategy performs better in terms of tracking the reference power with less deviation and a smoother response compared to 3O-SMC, C-SMC, and PI. This highlights the importance of selecting an appropriate control strategy based on the system's accuracy, stability, and robustness requirements under varying operating conditions.

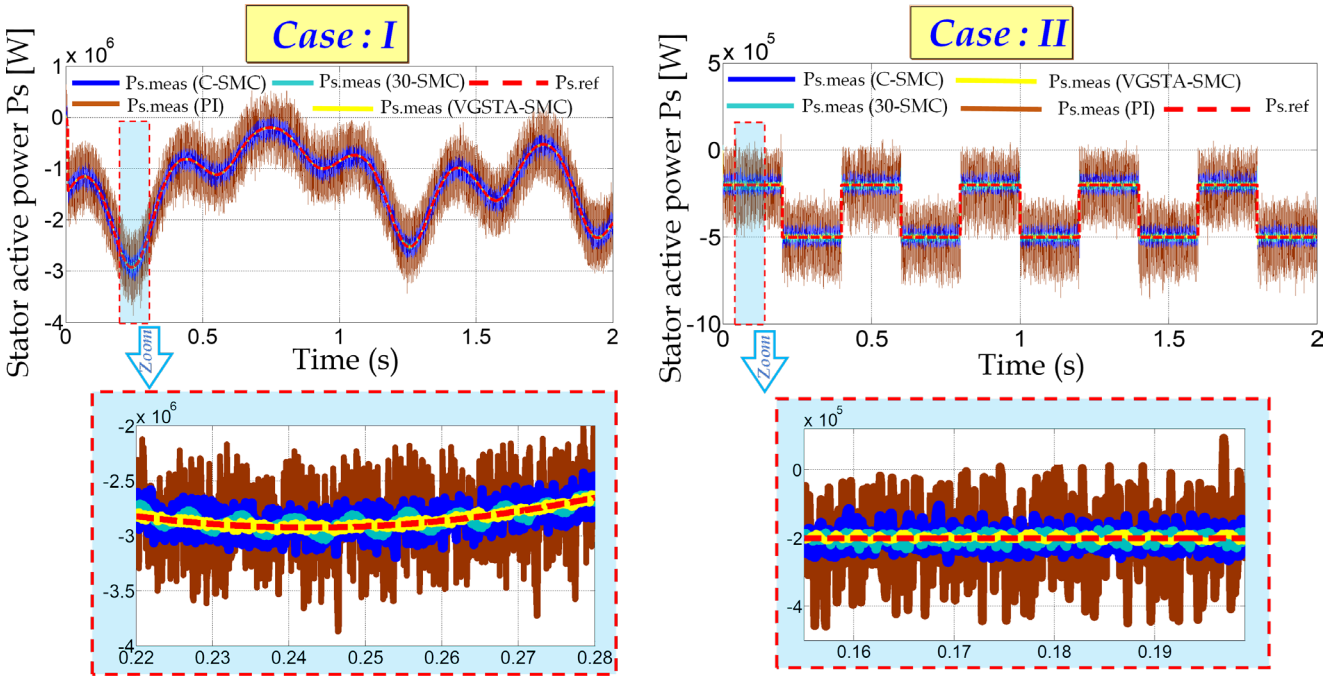

Fig. 13 Simulation results of the reference tracking test for both conventional and proposed control methods

6.4 Evaluating Control Strategies using Phase-Plane Trajectories

This simulation test aims to compare the performance of three control strategies (C-SMC, 3O-SMC, and VGSTA-SMC) by analyzing their phase-plane trajectories. By examining the trajectories, it is possible to determine which control strategy offers the best balance between stability, precision, and efficiency. The Fig. 14 compares the performance of three different control strategies: C-SMC, 3O-SMC, and VGSTA-SMC. Each plot represents the phase-plane trajectories of a controlled system under these strategies.

The C-SMC plot (Fig. 14(a)) exhibits a more scattered trajectory, reflecting classical sliding mode control's tendency for high-frequency oscillations or chattering and less smooth convergence to the desired state, which can be problematic in practical applications due to increased wear and energy consumption, resulting in less precise control compared to the other methods

In contrast, the 3O-SMC trajectory (Fig. 14(b)) is more consolidated and smoother, with quick convergence to a compact region, suggesting effective control with rapid stabilization, which makes it more efficient and reliable than C-SMC. This method enhances robustness and minimizes chattering by extending sliding mode control to higher-order derivatives. However, the VGSTA-SMC trajectory shows an initially wider spread of the trajectory, which converges to a smaller region over time. Thus, the proposed control is the smoothest and most regular compared to the C-SMC and 3O-SMC, showcasing minimal oscillations and the least chattering. This control strategy ensures fast and smooth convergence to the desired state with high robustness and stability. Therefore, while C-SMC is simple to implement, it is less desirable due to its high chattering. The 3O-SMC offers a good balance between simplicity and performance. In contrast, VGSTA-SMC (Fig. 14(c)) is ideal for applications requiring minimal chattering and high robustness, despite its more complex design and tuning requirements.

6.5 Robustness tests and performance comparison

Several factors, such as temperature, magnetic saturation of materials, harmonics, frequency changes, and others, can influence the parameters of an asynchronous generator in real-world applications. Therefore, in this test, the values of L_r and L_s are reduced by 10% to assess the impact of parameter variations on the performance of the proposed control strategy and to evaluate the system's performance and stability with and without MPPT. The Fig. 15 shows the simulation results for three different robust control strategies (C-SMC, 3O-SMC, and VGSTA-SMC) applied to a DFIG with variable parameters.

Through the simulation results, the three control strategies can maintain good performance even when the parameters of the DFIG change. However, the VGSTA-SMC controller has the best performance. We observe that the designed nonlinear controller VGSTA-SMC exhibits more robustness compared to both controllers C-SMC and 30-SMC. This is evident in the curves of active and reactive powers, which show a large number of oscillations at the energy level. These results also indicate that the VGSTA-SMC has the advantage of maintaining durability and reducing the chatter phenomenon caused by the signal function. Table 6 illustrates the numerical values of performance criteria for various controllers (PI, C-SMC, 3O-SMC, VGSTA-SMC). As shown in Table 7, a comprehensive and general comparison of these control devices

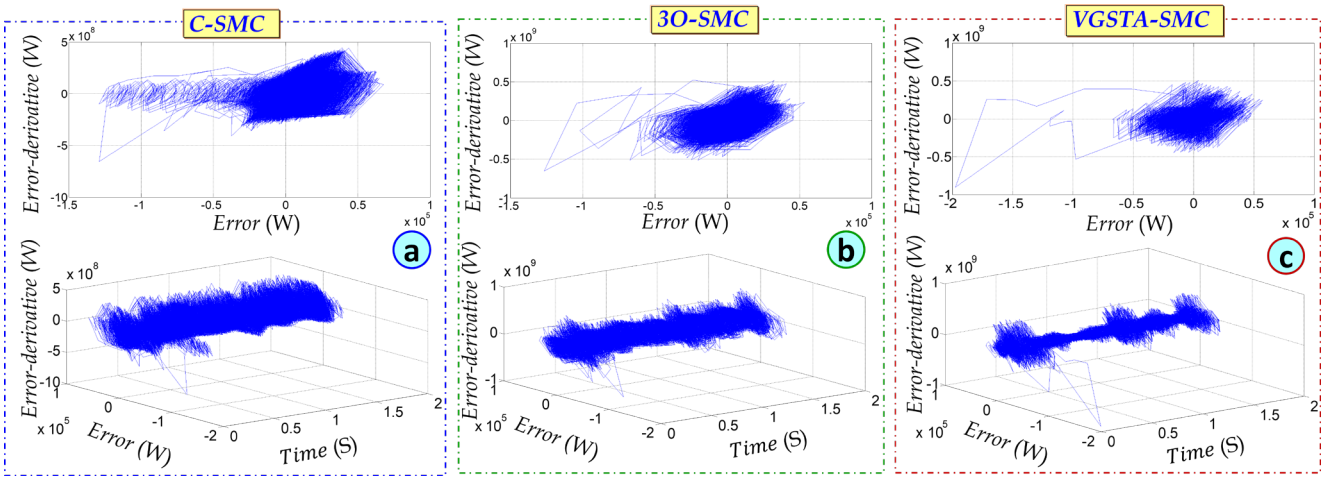

Fig. 14 The phase-plane trajectories of the different controllers in the wind energy system

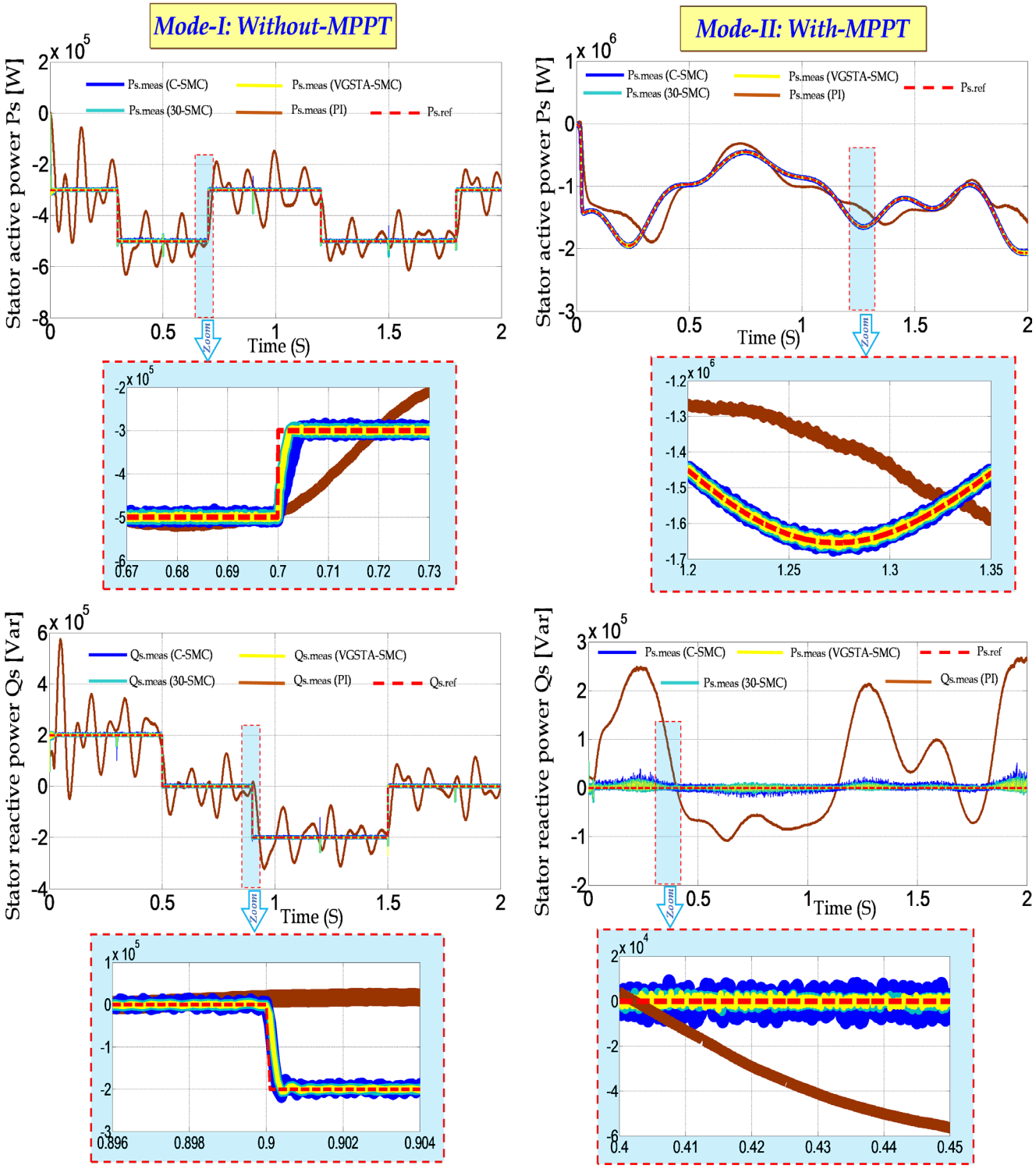

Fig. 15 Simulation results for power control under DFIG-variable parameters

is presented. To evaluate the performance of the proposed controller and demonstrate its advantages in terms of stability, robustness, and efficiency, the proposed controller is compared with other recently published control techniques, as shown in Table 8. An analysis of these results reveals that the proposed controller (VGSTA-SMC) exhibits significantly smaller IAE and ISE values compared to other controllers.

This indicates that the VGSTA-SMC produces minimal errors. Similarly, a trend of lower ITAE and ITSE values is observed for the same controller, suggesting its effectiveness in dealing with disturbances and rapid response to variations.

Table 6 Numerical values of performance criteria for different controllers

	Robustness test							
	Without MPPT				With MPPT			
Strategies	PI	C-SMC	3O-SMC	VGSTA-SMC	PI	C-SMC	3O-SMC	VGSTA-SMC
THD I_{s-abc}	2.56	0.95	0.3	0.26	2.69	1.14	1.11	1.09
THD I_{r-abc}	63.44	53.17	52.93	53.08	11.72	6.48	6.41	6.37
Respense time (ms)	2.1	1.5	0.9	0.6	1.9	1.38	0.7	0.3
Overshoot (%)	75	64	9	4	72	63	7	3
IAE (P_s)	9465	6904	2561	2549	1094	7168	4276	4266
IAE (Q_s)	8320	6061	2252	2230	1124	8266	3876	3847
ITAE (P_s)	6937	5765	1972	1964	1088	7137	4062	4089
ITAE (Q_s)	7498	5578	1921	1900	1104	8238	3727	3702
ISE (P_s)	$3.97 \cdot 10^8$	$2.834 \cdot 10^8$	$1.159 \cdot 10^8$	$1.153 \cdot 10^8$	$6.21 \cdot 10^7$	$4.56 \cdot 10^7$	$2.231 \cdot 10^7$	$2.191 \cdot 10^7$
ISE (Q_s)	$11.17 \cdot 10^7$	$8.906 \cdot 10^7$	$4.276 \cdot 10^7$	$4.641 \cdot 10^7$	$9.6 \cdot 10^7$	$7.152 \cdot 10^7$	$1.826 \cdot 10^7$	$1.79 \cdot 10^7$
ITSE (P_s)	$11.53 \cdot 10^7$	$8.428 \cdot 10^7$	$4.081 \cdot 10^7$	$3.955 \cdot 10^7$	$6.85 \cdot 10^7$	$4.587 \cdot 10^7$	$2.041 \cdot 10^7$	$2.11 \cdot 10^7$
ITSE (Q_s)	$7.58 \cdot 10^7$	$5.372 \cdot 10^7$	$2.58 \cdot 10^7$	$3.162 \cdot 10^7$	$9.9 \cdot 10^7$	$7.491 \cdot 10^7$	$1.682 \cdot 10^7$	$1.648 \cdot 10^7$

Table 7 Comparison of PI-controller, C-SMC, 3O-SMC, and VGSTA-SMC performance criteria for different controllers

	PI controller	C-SMC	3O-SMC	VGSTA-SMC
Approach	Linear	Nonlinear	Nonlinear	Nonlinear
Adaptability	Limited	Moderate	Moderate	High
Stability	Limited	Improved	Improved	Improved
Robustness	Limited	Moderate	High	High
Complexity	Low	Moderate	Moderate	Moderate to high
Tracking accuracy	Moderate	Moderate	High	High
Sensitivity to model uncertainties	High	Moderate	Moderate	Low
Implementation difficulty	Low	Moderate	Moderate	Moderate to high
Performance under disturbaces	Moderate	Moderate	High	High
Chattering effect	Low	Moderate	Moderate	Low to moderate
Applicability	Simple systems	Moderate complexity	Moderate to high complexity	High complexity

Table 8 Comparison between the proposed method and other controllers technologies published recently

Ref.	Year	Control technique	THD (%)	DFIG rated power	Reference tracking	Overshoot	Stator connection	Dynamic response	Robustness
[9]	2016	NFC/T2FLC-DPC	0.78	4.0 KW	++++	Neglected	Grid-connection	Excellent	High
[20]	2023	MRAC-I/OLDC	1.41	4.0 KW	++++	Neglected	Grid-connection	Very fast	High
[26]	2020	ST-FOTSMC	−−−	2.0 MW	++++	Neglected	Grid-connection	Excellent	−−−
[28]	2021	DFOC-TOSMC	1.42	1.5 MW	+++	Neglected ≈ 1.5%	Grid-connection	Excellent	High
[29]	2023	FOSTA	0.01	1.5 MW	++++	Neglected	Grid-connection	Excellent	High
[38]	2022	BCS-ALO	0.93	1.5 MW	++++	Neglected	Grid-connection	−−−−	−−−
[45]	2019	DPC-STA	1.66	1.5 MW	+++	−−−−	Grid-connection	Excellent	High

Table 8 Comparison between the proposed method and other controllers technologies published recently (continued)

Ref.	Year	Control technique	THD (%)	DFIG rated power	Reference tracking	Overshoot	Stator connection	Dynamic response	Robustness
[48]	2019	MRSMC	3.14	1.0 KW	−−−	−−−−	Grid-connection	−−−−	
[49]	2020	Fuzzy SOSMC	0.28	1.5 MW	+++	Neglected	Grid-connection	Excellent	High
[50]	2021	FOSMC	1.31	7.5 KW	++++	−−−−	Grid-connection	−−−−	High
[51]	2019	Fuzzy DTC.	1.73	1.5 KW	+++	−−−−	Grid-connection	−−−−	−−−
[52]	2021	NDVC-FPWM	0.13	1.5 MW	++++	Neglected	Grid-connection	Fast	Medium
[53]	2021	SYSTA-DRAPC	0.71	1.5 MW	+++	Neglected	Grid-connection	+++	High
[54]	2020	VM-DPC	1.7	2.0 MW	++++	−−−−	Grid-connection	+++	−−−
[55]	2023	TOSMC	0.83	10.0 KW	+++	Neglected	Grid-connection	Excellent	High
[56]	2019	FSMC	−−−	1.5 KW	++++	Neglected	−−−−	−−−−	High
[57]	2022	IP-DPC	3.62	4.5 KW	++++	Neglected	Stand-alone	Excellent	High
[58]	2016	FOC-Hysteresis	3.5	3.5 KW	+++	Neglected	Grid-connection	Fast	High
[59]	2021	ST-HODPSMC		1.5 KW	++++	Neglected	Grid-connection	−−−−	High
[60]	2024	ESOSM	−−−	5 MW	++++	Neglected	Grid-connection	Excellent	High
[61]	2021	VGSTSM		100 MW	+++	−−−−	Grid-connection	Fast	High
[62]	2022	IFOC-SSTA	0.10	1.5 MW	++++	−−−−	Grid-connection	Excellent	High
[63]	2019	STSMC	−−−	1.5 MW PMSG	+++	−−−−	Grid-connection	Excellent	Medium
[64]	2020	STA		7.5 kW		Neglected	Grid-connection	Fast	Medium
Proposed	−−	VGSTA-SMC	3.62	1.5 MW	++++	Neglected	Grid-connection	Excellent	High

7 Conclusion

In this paper, a study was conducted on a WECS based on a DFIG. The main objective of the proposed control was to enhance the system's performance despite variations of DFIG parameters and wind speed. The proposed VGSTA-SMC controller has exhibited excellent dynamic performance, ensuring high power quality even in the presence of wind speed fluctuations. Additionally, satisfactory improvements were provided, including a reduction in the total harmonic distortion (THD) of the stator current, minimization of static error, and minimization of the chattering phenomenon, in contrast to C-SMC and 3O-SMC controls. The validation was performed under *MATLAB*/*Simulink* environment.

The future trends of this work are various especially in terms of power converter; such as; multilevel converter, Matrix converter (MC) and Modular Matrix Converter (MMC) in order to improve the power quality delivered to the grid. Additionally, in order to improve the wind system performances, the hybrid power control such as: VGSTA-SMC based on an advanced Fuzzy Logic optimized by GA or PSO algorithm presents an excellent solution in the case of unbalanced grid voltage.

Nomenclature

DFIG	Double fed induction generator
MPPT	Maximum power point tracking
FOC	Field-oriented control
C-SMC	Conventional Sliding Mode Control
3O-SMC	Third Order Sliding Mode Control
VGSTA	Variable Gain Super Twisting Algorithm
FOSTA	Fractional-Order Super Twisting Algorithm
FOSMC	Fractional-Order Sliding Mode Control
DFOC-TOSMC	Direct Field-Oriented Control-Third Order Sliding Mode Control
MRSMC	Multi-resonant-based sliding mode control
VM-DPC	Voltage modulated direct power control
Fuzzy SMC	Fuzzy Sliding Mode Control
Fuzzy DTC	Fuzzy Direct Torque Control
DPC-STA	Direct Power Control-Super Twisting Algorithm
ST-FOTSMC	Super Twisting Fractional Order Terminal Sliding Mode Control
NDVC-FPWM	Direct vector command-?
SYSTA-DRAPC	Synergetic-super twisting algorithms-direct reactive and active power control
ST-FOTSMC	Super twisting fractional order terminal sliding mode control
MRAC	Model Reference Adaptive Control
MRAS	Model Reference Adaptive System
IP-DPC	Integral Proportional- Direct Power Control
I/OLDC	Input/Output Linearizing and Decoupling Control
NFC	Neuro-Fuzzy Control
T2FLC	Type-2 Fuzzy Logic Control
ST-HODPSMC	Super Twisting Based High Order Direct Power Sliding Mode Control

References

[1] Tahiri, F., Harrouz, A., Dumbrava, V., Badoud, A., Alnatoor, M. "Non-linear controls for robustness investigation of PMSG-based wind turbine", University Politehnica of Bucharest Scientific Bulletin Series C - Electrical Engineering and Computer Science, 84(2), pp. 377–396, 2022. [online] Available at: https://www.scientificbulletin.upb.ro/rev_docs_arhiva/full98a_253492.pdf [Accessed: 07 July 2024]

[2] Hassan, Q., Viktor, P., Al-Musawi, T. J., Ali, B. M., Algburi, S., Alzoubi, H. M., Al-Jiboory, K. A., Sameen, A. Z., Salman, H. M., Jaszczur, M. "The renewable energy role in the global energy Transformations", Renewable Energy Focus, 48, 100545, 2024. https://doi.org/10.1016/j.ref.2024.100545

[3] Yessef, M., Taoussi, M., Bossoufi, B., Lagrioui, A. "Robust Control of a Wind Conversion System Based on a Doubly Fed Induction Generator: A Comparison Between Adaptive Backstepping and Integral Sliding Mode Controllers", In: Motahhir, S., Bossoufi, B. (eds.) Digital Technologies and Applications. Proceedings of ICDTA'22, Fez, Morocco, 2022, pp. 722–732. ISBN 978-3-031-01941-8 https://doi.org/10.1007/978-3-031-01942-5_72

[4] Bossoufi, B., Karim, M., Taoussi, M., Aroussi, H., Bouderbala, M., Ddeblecker, O., Motahhir, S., Nayyar, A., Mihammed, A., Alzain, A. "Rooted Tree Optimization for the Backstepping Power Control of a Doubly Fed Induction Generator Wind Turbine: dSPACE Implementation", IEEE Access, 9, pp. 26512– 26522, 2021. https://doi.org/10.1109/ACCESS.2021.3057123

[5] Patel, R., Hafiz, F., Swain, A., Ukil, A. "Nonlinear rotor side converter control of DFIG based wind energy system", Electric Power Systems Research, 198(2), 107358, 2021. https://doi.org/10.1016/j.epsr.2021.107358

[6] Kabir, M., Sree, N., Khatod, K., Katekar, V., Deshmukh, S. "Wind energy and its link to sustainability in developing countries", In: Khan, I. (ed.) Renewable Energy and Sustainability, Elsevier, 2022, pp. 135–178. ISBN 978-0-323-88668-0 https://doi.org/10.1016/B978-0-323-88668-0.00008-5

[7] Mahroug, R., Matallah, M., Abudura, S. "Modeling of wind turbine based on dual DFIG generators", International Journal of Power Electronics and Drive Systems (IJPEDS), 13(2), pp. 1170–1185, 2022. https://doi.org/10.11591/ijpeds.v13.i2.pp1170-1185

[8] Nian, H., Cheng, P., Zhu, Z. Q. "Coordinated Direct Power Control of DFIG System without Locked Loop under Unbalanced Grid Voltage Conditions", IEEE Transactions on Power Electronics, 31(4), pp. 2905–2918, 2016. https://doi.org/10.1109/TPEL.2015.2453127

[9] Amrane, F., Chaiba, A. "A novel direct power control for grid connected doubly fed induction generator based on hybrid artificial intelligent control with space vector modulation", Revue Roumaine des Sciences Techniques – Serie Électrotechnique et Énergétique, 61(3), pp. 263–268, 2016. [online] Available at: http://revue.elth.pub.ro/index.php?action=details&id=597 [Accessed: 07 July 2024]

[10] Djeriri, Y. "Robust Second Order Sliding Mode Control of Doubly-Fed Induction Generator for Wind Energy Conversion System", Acta Electrotechnica et Informatica, 20(3), pp. 30–38, 2020. https://doi.org/10.15546/aeei-2020-0017

[11] Nekoukar, V., Erfanian, A. "Adaptive fuzzy terminal sliding mode control for a class of MIMO uncertain nonlinear systems", Fuzzy Sets and Systems, 179(1), pp. 34–49, 2011. https://doi.org/10.1016/j.fss.2011.05.009

[12] Reyad, A. F., László, S. "Predictive Direct Torque Control of Switched Reluctance Motor for Electric Vehicles Drives", Periodica Polytechnica Electrical Engineering and Computer Science, 64(3), pp. 264–273, 2020. https://doi.org/10.3311/PPee.15496

[13] Mossa, M. A., Abdelhamid, M. K., Hassan, A. A. "Enhancing the Dynamic Performance of a Wind Driven Grid Connected DFIG Using an Effective Control Approach", In: IEEE Conference on Power Electronics and Renewable Energy (CPERE), Luxor, Egypt, 2023, pp. 1–7. ISBN 978-1-6654-5233-5 https://doi.org/10.1109/CPERE56564.2023.10119614

[14] Abdeddaim, S., Betka, A., Drid, S., Becherif, M. "Implementation of MRAC controller of a DFIG based variable speed grid connected wind turbine", Energy Conversion and Management, 79, pp. 281–288, 2014. https://doi.org/10.1016/j.enconman.2013.12.003

[15] Mosaad, M. I. "Model reference adaptive control of STATCOM for grid integration of wind energy systems", IET Electric Power Applications, 12(5), pp. 605–613, 2018. https://doi.org/10.1049/iet-epa.2017.0662

[16] Cárdenas, R., Peña, R., Proboste, J., Asher, G., Clare, J. "MRAS Observer for Sensorless Control of Standalone Doubly Fed Induction Generators", IEEE Transactions on Energy Conversion, 20(4), pp. 710–718, 2005. https://doi.org/10.1109/TEC.2005.847965

[17] Cárdenas, R., Peña, R., Asher, G., Clare, J., Cartes, J. "MRAS Observer for Doubly Fed Induction Machines", IEEE Transactions on Energy Conversion, 19(2), pp. 467–468, 2004. https://doi.org/10.1109/TEC.2004.827052

[18] Cárdenas, R., Peña, R., Clare, J., Asher, G., Proboste, J. "MRAS Observers for Sensorless Control of Doubly-Fed Induction Generators", IEEE Transactions on Power Electronics, 23(3), pp. 1075–1084, 2008. https://doi.org/10.1109/TPEL.2008.921189

[19] Mbukani, M. W. K., Gitau, M. N., Naidoo, R. "An SMC-MRAS Speed Estimator for Sensor-Less Control of DFIG Systems in Wind Turbine Applications", Energies, 16(6), 2633, 2023. https://doi.org/10.3390/en16062633

[20] F. Amrane, F., Chaiba, A., Francois, B. "Improved adaptative non-linear control for variable speed wind-turbine fed by direct matrix converter", Revue Roumaine des Sciences Techniques – Série Électrotechnique et Énergétique, 68(1), pp. 58–64, 2023. https://doi.org/10.59277/RRST-EE.2023.68.1.10

[21] Elmouhi, N., Essadki, A., Elaimani, H. "Robust control of wind turbine based on doubly-fed induction generator optimized by genetic algorithm", International Journal of Power Electronics and Drive System (IJPEDS), 13(2), pp. 674–688, 2022. https://doi.org/10.11591/ijpeds.v13.i2.pp674-688

[22] Şeker, M., Zergeroğlu, E., Tatlicioğlu, E. "Non-linear control of variable-speed wind turbines with permanent magnet synchronous generators: a robust backstepping approach", International Journal of Systems Science, 47(2), pp. 420–432, 2016. https://doi.org/10.1080/00207721.2013.834087

[23] Itouchene, H., Amrane, F., Boudries, Z. "Robust Control of DFIG Wind Turbines in Sub/Super-Synchronous Operation Using Integral Backstepping Controller", Journal of Renewable Energies, 1(1), pp. 23–31, 2024. https://doi.org/10.54966/jreen.v1i1.1170

[24] Boudjema, Z., Taleb, R., Djeriri, Y., Yahdou, A. "A novel direct torque control using second order continuous sliding mode of a doubly fed induction generator for a wind energy conversion system", Turkish Journal of Electrical Engineering and Computer Sciences, 25(2), pp. 965–975, 2017. https://doi.org/10.3906/elk-1510-89

[25] Sami, I., Ullah, S.H., Ul-amin, S., Al-durra, A., Ullah, N., Suk-ro, J. "Convergence Enhancement of Super-Twisting Sliding Mode Control Using Artificial Neural Network for DFIG-Based Wind Energy Conversion Systems", IEEE Access, 10, pp. 97625–97641, 2022. https://doi.org/10.1109/ACCESS.2022.3205632

[26] Sami, I., Ullah, S., Ali, Z., Ullah, N., Jong-Suk, Ro, J.-S. "A Super Twisting Fractional Order Terminal Sliding Mode Control for DFIG-Based Wind Energy Conversion System", Energies, 13(9), 2158, 2020. https://doi.org/10.3390/en13092158

[27] Gonzalez, T., Moreno, J., Fridman, L. "Variable Gain Super-Twisting Sliding Mode Control", IEEE Transactions on Automatic Control, 57(8), pp. 2100–2105, 2012. https://doi.org/10.1109/TAC.2011.2179878

[28] Benbouhenni, H., Bizon, N. "Third-Order Sliding Mode Applied to the Direct Field-Oriented Control of the Asynchronous Generator for Variable-Speed Contra-Rotating Wind Turbine Generation Systems", Energies, 14(18), 5877, 2021. https://doi.org/10.3390/en14185877

[29] Gasmi, H., Benbouhenni, H., Mendaci, S., Colak, I. "A new scheme of the fractional-order super twisting algorithm for asynchronous generator-based wind turbine", Energy Reports, 9, pp. 6311–6327, 2023. https://doi.org/10.1016/j.egyr.2023.05.267

[30] Amara, M., Mazouar, A., Sayah, H. "Enhanced control of wind energy conversion system based on DFIG using adaptive super twisting controllers", Journal Européen des Systèmes Automatisés, 55(1), pp. 109–117, 2022. https://doi.org/10.18280/jesa.550111

[31] Evangelista, E., Puleston, P., Valenciaga, F., Dávila, A. "Variable gains super-twisting control for wind energy conversion optimization", In: 11th International Workshop on Variable Structure Systems (VSS), Mexico City, Mexico, 2010, pp. 50–55. https://doi.org/10.1109/VSS.2010.5544713

[32] Deep, S., Sarkar, A., Ghawat, M., Rajak, M. K. "Estimation of the wind energy potential for coastal locations in India using the Weibull model", Renewable Energy, 161, pp. 319–339, 2020. https://doi.org/10.1016/j.renene.2020.07.054

[33] Manwell, J. F., McGowan, J. G., Rogers, A. L. "Aerodynamics of Wind Turbines", In: Wind Energy Explained: Theory, Design and Application, John Wiley & Sons, Ltd, 2009, pp. 91–155. ISBN 9780470015001
https://doi.org/10.1002/9781119994367.ch3

[34] Chetouani, E., Errami, Y., Obbadi, A., Sahnoun, S. "Self-adapting PI controller for grid-connected DFIG wind turbines based on recurrent neural network optimization control under unbalanced grid faults", Electric Power Systems Research, 214, 108829, 2023.
https://doi.org/10.1016/j.epsr.2022.108829

[35] Yin, X.-X., Lin, Y.-G., Li, W., Gu, Y.-J., Wang, X.-J., Lei, P.-F. "Design, modeling and implementation of a novel pitch angle control system for wind turbine", Renewable Energy, 81, pp. 599–608, 2015.
https://doi.org/10.1016/j.renene.2015.03.042

[36] Bouregba, H., Hachemi, M., Bey, M., Hamidat, A. "Stability analysis of the pitch angle control of large wind turbines using different controller strategies", Advances in Mechanical Engineering, 14(11), pp. 1–18, 2022.
https://doi.org/10.1177/16878132221139926

[37] Amrane, F., Chaiba, A., Chebabhi, A. "Improvement Performances of Doubly Fed Induction Generator via MPPT Strategy using Model Reference Adaptive Control based on Direct Power Control with Space Vector Modulation", Journal of Electrical Engineering, 16(3), pp. 218–225, 2016. [online] Available at: https://www.semanticscholar.org/paper/Improvement-performances-of-Doubly-Fed-Induction-Amrane/6551848a9c6cbe01ca0ae269a65e644a75f2d2e7 [Accessed: 07 July 2024]

[38] Zeghdi, Z., Barazane, L., Bekakra, Y., Larabi, A. "Improved Backstepping Control of a DFIG based Wind Energy Conversion System using Anti Lion Optimizer Algorithm", Periodica Polytechnic Electrical Engineering and Computer Science, 66(1), pp. 43–59, 2022.
https://doi.org/10.3311/PPee.18716

[39] Amrane, F., Chaiba, A. "Improved Indirect Power Control (IDPC) of Wind Energy Conversion Systems (WECS)", Bentham Science Publishers Pte. Ltd., 2019. ISBN 9789811412677
https://doi.org/10.2174/9789811412677190101

[40] Boubzizi, H., Abid, A., El-Hajjaji, M., Chaabane, M. "Comparative study of three types of controllers for DFIG in wind energy conversion system", Protection and Control of Modern Power Systems, 3(1), 21, 2018.
https://doi.org/10.1186/s41601-018-0096-y

[41] Chetouani, E., Errami, Y., Obbadi, A., Sahnoun, S. "Optimal tuning of pi controllers using adaptive particle swarm optimization for doubly-fed induction generator connected to the grid during a voltage dip", Bulletin of Electrical Engineering and Informatics. 10(5), pp. 2367–2376, 2021.
https://doi.org/10.11591/eei.v10i5.2843

[42] Hua, C., Chen, J., Guan, X. "Adaptive prescribed performance control of QUAVs with unknown time-varying payload and wind gust disturbance", Journal of the Franklin Institute, 355(14), pp. 6323–6338, 2018.
https://doi.org/10.1016/j.jfranklin.2018.05.062

[43] Beltran, B., Ahmed-Ali, T., Benbouzid, M. "Sliding Mode Power Control of Variable-Speed Wind Energy Conversion Systems", IEEE Transactions on Energy Conversion, 23(2), pp. 551–558, 2008.
https://doi.org/10.1109/TEC.2007.914163

[44] Bartolini, G., Ferrara, A., Usai, E. "Chattering avoidance by second order sliding mode control", IEEE Transactions on Automatic Control, 43(2), pp. 241–246, 1998.
https://doi.org/10.1109/9.661074

[45] Yaichi, I., Semmah, A., Wira, P., Djeriri, Y. "Super-twisting sliding mode control of a doubly-fed induction generator based on the SVM strategy", Periodica Polytechnica Electrical Engineering and Computer Science, 63(3), pp. 178–190, 2019.
https://doi.org/10.3311/PPee.13726

[46] Herizi, A., Rouabhi, R. "Hybrid Control Using Sliding Mode Control with Interval Type-2 Fuzzy Controller of a Doubly Fed Induction Generator for Wind Energy Conversion", International Journal of Intelligent Engineering and Systems, 15(1), pp. 549–562, 2022.
https://doi.org/10.22266/ijies2022.0228.50

[47] Xuan-Mung, N,. Nguyen, N. P., Pham, D. P., Dao, N.-N,. Nguyen, H. T., Ha Le Nhu Ngoc, T., Vu, M. T., Hong, S. K. "Novel gain-tuning for sliding mode control of second-order mechanical systems: theory and experiments", Scientifc Reports, 13(1), 10541, 2023.
https://doi.org/10.1038/s41598-023-37562-7

[48] Quan, Y., Hang, L., He, Y., Zhang, Y. "Multi-Resonant-Based Sliding Mode Control of DFIG-Based Wind System under Unbalanced and Harmonic Network Conditions", Applied Sciences, 9(6), 1124, 2019.
https://doi.org/10.3390/app9061124

[49] Alhato, M. M., Bouallègue, S., Rezk, H. "Modeling and Performance Improvement of Direct Power Control of Doubly-Fed Induction Generator Based Wind Turbine through Second-Order Sliding Mode Control Approach", Mathematics, 8(11), 2012, 2020.
https://doi.org/10.3390/math8112012

[50] Beniss, M. A., El-Moussaoui, H., Lamhamdi, T., El-Markhi, H. "Improvement of power quality injected into the grid by using a FOSMC-DPC for doubly fed induction generator", International Journal of intelligent Engineering & Systems, 14(2), pp. 556–567, 2021.
https://doi.org/10.22266/ijies2021.0430.50

[51] El-Ouanjli, N., Motahhir, S., Derouich, A., El-Ghzizal, A., Chebabhi, A., Taoussi, M. "Improved DTC strategy of doubly fed induction motor using fuzzy logic controller", Energy Reports, 5, pp. 271–279, 2019.
https://doi.org/10.1016/j.egyr.2019.02.001

[52] Benbouhenni, H., Bizon, N. "Advanced Direct Vector Control Method for Optimizing the Operation of a Double-Powered Induction Generator-Based Dual-Rotor Wind Turbine System", Engineering Mathematics, 9(19), 2403, 2021.
https://doi.org/10.3390/math9192403

[53] Benbouhenni, H., Lemdani, S. "Combining synergetic control and super twisting algorithm to reduce the active power undulations of doubly fed induction generator for dual-rotor wind turbine system", Electrical Engineering & Electromechanics, 621(3), pp. 8–17, 2021.
https://doi.org/10.20998/2074-272X.2021.3.02

[54] Cheng, P., Wu, C., Ning, F., He, J. "Voltage Modulated DPC Strategy of DFIG Using Extended Power Theory under Unbalanced Grid Voltage Conditions", Energies, 13(22), 6077, 2020.
https://doi.org/10.3390/en13226077

[55] Kadi, S., Benbouhenni, H., Abdelkarim, E., Imarazene, K., Berkouk, E. M. "Implementation of third-order sliding mode for power control and maximum power point tracking in DFIG-based wind energy systems", Energy Reports, 10, pp. 3561–3579, 2023.
https://doi.org/10.1016/j.egyr.2023.09.187

[56] Mechernene, A., Loucif, M., Zerikat, M. "Induction motor control based on a fuzzy sliding mode approach", Revue Roumaine des Sciences Techniques – Serie Électrotechnique et Énergétique, 64(1), pp. 39–44, 2019. [online] Available at: http://revue.elth.pub.ro/index.php?action=details&id=814 [Accessed: 07 July 2024]

[57] Amrane, F., Francois, B., Chaiba, A. "Experimental Investigation of Efficient and Simple Wind-Turbine based on DFIG-Direct Power Control using LCL-Filter for Stand-alone Mode", ISA Transactions, 125, pp. 631–664, 2022.
https://doi.org/10.1016/j.isatra.2021.07.008

[58] Amrane, F., Chaiba, A., Babes, B. E., Mekhilef, S. "Design and Implementation of High-Performance Field Oriented Control for Grid-Connected Doubly Fed Induction Generator via Hysteresis Rotor Current Controller", Revue Roumaine des Science Techniques – Serie Électrotechnique et Énergétique, 61(4), pp. 319–324, 2016. [online] Available at: http://revue.elth.pub.ro/index.php?action=details&id=609 [Accessed: 07 July 2024]

[59] Dekali, Z., Baghli, L., Boumediene, A. "Improved Super Twisting Based High Order Direct Power Sliding Mode Control of a Connected DFIG Variable Speed Wind Turbine", Periodica Polytechnica Electrical Engineering and Computer Science, 65(4), pp. 352–372, 2021.
https://doi.org/10.3311/PPee.17989

[60] Ma, R., Siaw, F. L., Thio, T. H. G., Yang, W. "New Adaptive Super-Twisting Extended-State Observer-Based Sliding Mode Scheme with Application to FOWT Pitch Control", Journal of Marine Science and Engineering, 12(6), 902, 2024.
https://doi.org/10.3390/jmse12060902

[61] Ma, R., Haw, Y., Pan, W. "Variable-Gain Super-Twisting Sliding Mode Damping Control of Series-Compensated DFIG-Based Wind Power System for SSCI Mitigation", Energies, 14(2), 382, 2021.
https://doi.org/10.3390/en14020382

[62] Benbouhenni, H., Bizon, N., Colak, I., Thounthong, P., Takorabet, N. "Simplified Super Twisting Sliding Mode Approaches of the Double-Powered Induction Generator-Based Multi-Rotor Wind Turbine System", Sustainability, 14(9), 5014, 2022.
https://doi.org/10.3390/su14095014

[63] Nasiri, M., Mobayen, S., Min Zhu, Q. "Super-Twisting Sliding Mode Control for Gearless PMSG-Based Wind Turbine", Complexity, 2019(1), 6141607, 2022.
https://doi.org/10.1155/2019/6141607

[64] Kelkoul, B., Boumediene, A. "Stability analysis and study between Classical Sliding Mode Control (SMC) and Super Twisting Algorithm (STA) for Doubly Fed Induction Generator (DFIG) under Wind turbine", Energy, 214, 118871, 2020.
https://doi.org/10.1016/j.energy.2020.118871

Appendix

Table A1 The turbine parameters

$R = 35.25$ m	Blade radius
$n_p = 3$	Number of blades
$G = 90$	Gearbox ratio
$J = 10^3$ kg m^2	Inertia
$f_r = 2.4 \cdot 10^{-3}$ N m S^{-1}	Viscous friction coefficient
V =12 m/s	Nominal wind speed

Table A2 DFIG parameters

$P_n = 1.5$ MW	Rated power
$V_r = 225$ V	Rotor rated voltage
$V_s/U_s = 398/690$ V	Stator rated voltage
$I_n = 1900$ A	Rated current
$f = 50$ Hz	Stator rated frequency
$L_m = 13.5$ mH	Mutual inductance
$L_s = 13.7$ mH	Stator inductance
$L_r = 13.6$ mH	Rotor inductance
$R_s = 12$ mΩ	Stator resistance
$R_r = 21$ mΩ	Rotor resistance
$P = 2$	Number of Pole pairs